Lithos 110 (2009) 277–293

Contents lists available at ScienceDirect

Lithos

journal homepage: www.elsevier.com/locate/lithos

Adakitic signature formed by fractional crystallization: An interpretation for the Neo-Proterozoic meta-plagiogranites of the NE Jiangxi ophiolitic mélange belt, South China

Jun Gao [a,*], Reiner Klemd [b], Lingli Long [c], Xianming Xiong [d], Qing Qian [a]

[a] Key Laboratory of Mineral Resources, Institute of Geology and Geophysics, Chinese Academy of Sciences, PO Box 9825, Beijing 100029, China
[b] GeoZentrum Nordbayern, Universität Erlangen, Schlossgarten 5a, 91054 Erlangen, Germany
[c] Beijing Institute of Geology for Mineral Resources, Beijing 100012, China
[d] College of Resources and Environmental Engineering, Guizhou University, Guiyang 550003, China

ARTICLE INFO

Article history:
Received 1 August 2008
Accepted 21 January 2009
Available online 3 February 2009

Keywords:
Adakitic signature
Fractional crystallization
Neo-Proterozoic meta-plagiogranites
The NE Jiangxi ophiolitic mélange belt

ABSTRACT

The low-temperature/high-pressure metamorphic rocks which are exposed as exotic blocks within the serpentinite matrix of the NE Jiangxi ophiolitic mélange belt consist of enclave-bearing and -free meta-plagiogranites. Both rock types are characterized by a metamorphic mineral assemblage consisting of Ab-rich plagioclase + quartz +/− clinopyroxene + amphibole while rutile, titanite and zircon occur as accessories. The former primary magmatic mineral parageneses for the meta-mafic enclaves and the meta-plagiogranites are similar and consist of An-rich-plagioclase + hornblende + ilmenite + monazite + apatite. However, the Ab-rich plagioclase abundance of the meta-mafic enclave is much lower and the hornblende and accessory mineral abundances are higher compared with those of the meta-plagiogranite host rocks. Meta-plagiogranites with mafic enclaves have a chemical composition similar to that of typical adakites, with elevated Al_2O_3 (15.86 wt.%), Mg# (53.5) and Sr contents (485 ppm) and a positive Eu anomaly. The rare earth element patterns are highly fractionated with ($(La/Yb)_N$>12) and low Y (<4 ppm) and Yb (<0.4 ppm). The mafic enclave has a basaltic composition with a negative Eu anomaly and has *ca.* 10 times higher HREE and Y concentrations than the plagiogranite host rocks. Enclave-free meta-plagiogranites also have high Al_2O_3 (16.08 wt.%), Na_2O (8.88 wt.%) and Mg# (52.3) values without obvious Eu enrichment or depletion. The Y and Yb concentrations (13 and 1.33 ppm, respectively) are higher than those of the enclave-bearing meta-plagiogranites and slightly lower than those of the mafic enclave. Zircon of the enclave-bearing meta-plagiogranites gives a weighted mean $^{206}Pb/^{238}U$ crystallization age of 970 ± 21 Ma. These meta-plagiogranites have low $^{87}Sr/^{86}Sr$ value of ~0.7026 and high εNd(970 Ma) of 6.6 to 7.4. The meta-mafic enclave has a similar isotope composition with a $^{87}Sr/^{86}Sr$ value of 0.7023 and a $\varepsilon Nd(T)$ of 6.2. The enclave-free meta-plagiogranites have relatively higher $^{87}Sr/^{86}Sr$ (0.7037 to 0.7045) and lower $\varepsilon Nd(T)$ (−1.22 to −1.28) values. Trace element data of the minerals and whole rocks suggest that Y and Yb are hosted in amphibole, apatite and titanite, Nb in rutile, titanite and amphibole and Sr mainly in plagioclase. Petrographic and geochemical evidence indicates that the meta-mafic enclaves are 'schlieren', which formed by the early crystallization of accessory minerals and hornblende, in the meta-plagiogranites. The adakitic signature of enclave-bearing meta-plagiogranites is interpreted to be due to fractional crystallization of hornblende and accessory minerals such as apatite and ilmenite from the parent magmas, instead of the melting of subducted, spilitized oceanic crust with residual garnet and amphibole. The plagiogranitic magma may have evolved from a basaltic parent magma which had originated in the mantle wedge beneath the Neoproterozoic (*ca.* 970 Ma) island arc along the southern margin of the Yangtze block.

1. Introduction

The origin of igneous rocks with an adakitic signature (elevated La/Yb, high Sr (>400 ppm) and Al_2O_3 contents (≥15%), high Sr/Y ratios, Y ≤ 18 ppm and Yb ≤ 1.9 ppm; Defant and Drummond, 1990; Drummond and Defant, 1990; Drummond et al., 1996) is the subject of an ongoing debate among the geoscientific community. Originally, the generation of adakitic magmas was restricted to subduction of very young (<25 Ma) oceanic lithosphere (Defant and Drummond, 1990). However, many adakitic igneous rocks are exposed in convergent margins where subducting slabs are considered to be too old to have been derived by partial melting in the subduction zone. In such cases alternative

* Corresponding author.
E-mail addresses: gaojun@mail.igcas.ac.cn (J. Gao), klemd@geol.uni-erlangen.de (R. Klemd).

0024-4937/$ – see front matter © 2009 Elsevier B.V. All rights reserved.
doi:10.1016/j.lithos.2009.01.009

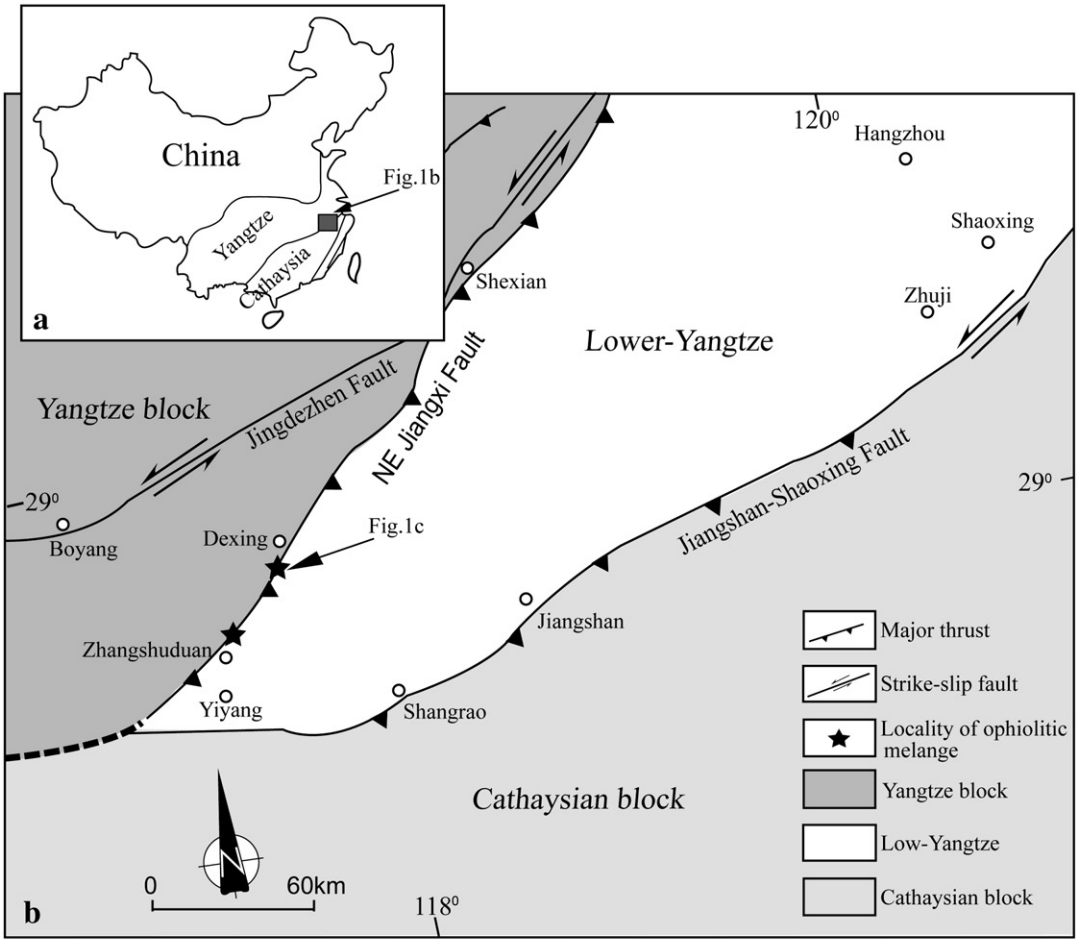
China
Fig.1b
Yangtze
Cathaysia
a
120°
Hangzhou
Shaoxing
Shexian
Zhuji
Lower-Yangtze
Yangtze block
Jingdezhen Fault
NE Jiangxi Fault
Jiangshan-Shaoxing Fault
29°
Boyang
Dexing
Fig.1c
Zhangshuduan
Yiyang
Jiangshan
Shangrao
Major thrust
Strike-slip fault
Locality of ophiolitic melange
Yangtze block
Low-Yangtze
Cathaysian block
Cathaysian block
0
60km
118°
b

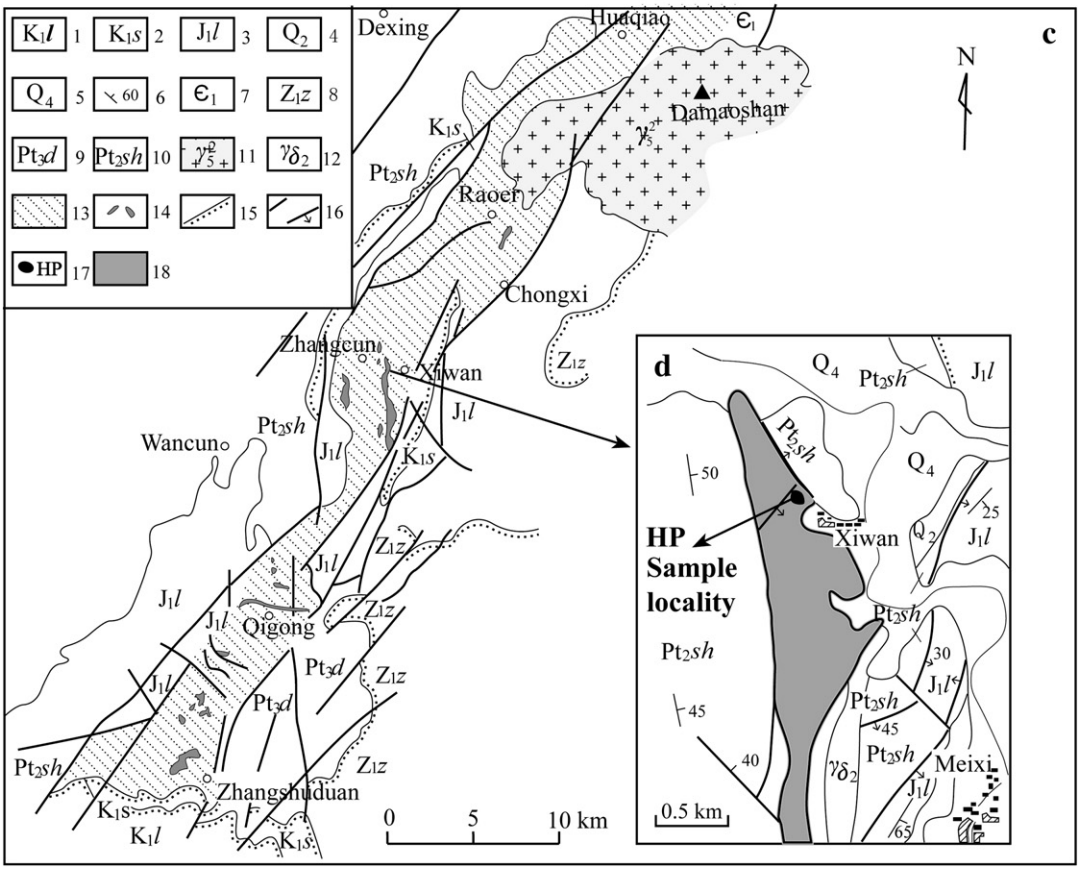
K1l 1
K1s 2
J1l 3
Q2 4
Q4 5
60 6
ϵ1 7
Z1z 8
Pt3d 9
Pt2sh 10
11
γδ2 12
13
14
15
16
HP 17
18
Dexing
Huaqiao
ϵ1
Damaoshan
K1s
Pt2sh
Raoer
Chongxi
Zhangcun
Xiwan
Z1z
J1l
Wancun
Pt2sh
K1s
Qigong
Pt3d
Zhangshuduan
K1l
K1s
0 5 10 km
N
c
d
Q4
Pt2sh
J1l
50
HP
Sample
locality
Xiwan
25
30
45
40
Meixi
0.5 km
65

geodynamic models, such as subduction of the leading edges of newly subducted slabs (Sajona et al., 1993; Yogodzinski et al., 2001) or slab-window margins (Thorkelson and Breitsprecher, 2005), highly oblique convergence (Yogodzinski and Kelemen, 1998) and flat subduction (Gutscher et al., 2000) have been proposed in order to provide mechanisms for the melting of cold oceanic crust. Models favoring the melting of mafic, mantle-derived materials underplated at the base of lower crust have also been proposed (e.g. Atherton and Petford, 1993; Zhao et al., 2008).

In addition to the melting of young oceanic crust or mafic material underplated at the lower crust, crystal fractionation of the requisite mineral assemblage from wet basaltic magmas has also been suggested to produce evolved magmas with adakitic chemical characteristics (Castillo et al., 1999; Garrison and Davidson, 2003; Kleinhanns et al., 2003; Prouteau and Scaillet, 2003; Castillo, 2006; Macpherson et al., 2006; Rodriguez et al., 2007; Petrone and Ferrari, 2008).

In either melting or crystal fractionation models, the HREE (i.e. Yb) and Y-carrier minerals garnet and amphibole were suggested to be responsible for the creation of the typical chemical characteristic of adakites (e.g. Defant and Drummond, 1990; Martin, 1999; Macpherson et al., 2006; Rodriguez et al., 2007). Here we present the petrography, mineral and whole-rock chemistry of Neo-Proterozoic meta-plagiogranites with an adakitic signature from the NE Jiangxi ophiolitic mélange belt, South China (Fig. 1). Li and Li (2003) suggested low degrees of partial melting of subducted, spilitized oceanic crust at pressures high enough to stabilize garnet and amphibole to be responsible for the formation of these adakitic meta-plagiogranites. We alternatively propose that partial melting was not responsible for the adakitic chemical signature, instead, fractionation of hornblende and accessory minerals such as apatite and ilmenite lead to its development.

2. Tectonic setting

The NE Jiangxi ophiolitic mélange belt extends between the Yangtze and the Cathaysian (also called South China) blocks for about 200 km in a NE–SW direction (Fig. 1a, b and c; Shu and Zhou, 1988; Shu et al., 1995; Chen et al., 1991; Xiao and He, 2005). The ophiolitic mélange occurs near the southern margin of the Yangtze plate and was tectonically emplaced within Banxi low-grade metamorphic slates and phyllites (Chen et al., 1991; Xu et al., 1992). It mainly consists of exotic blocks (gabbro, basalt, diabase, diorite and chert) as well as some low-temperature/high-pressure (LT/HP) metamorphic granitic blocks enclosed within a serpentinite matrix (Zhou, 1989, 1997). Sm-Nd isochron ages of 930 ± 34 Ma, 1154 ± 43 Ma and 1024 ± 30 Ma were obtained for whole rock samples from the igneous blocks (Xu and Qiao, 1989; Zhou, 1989; Zhou and Zhao, 1991). Additionally, Sm–Nd mineral (plagioclase and pyroxene) and whole rock isochron ages of 1034 ± 24 Ma and 935 ± 10 Ma were derived for the gabbroic blocks (Chen et al., 1991). A K–Ar age of 866 ± 14 Ma and an Ar–Ar plateau age of 799 Ma were obtained for amphibole from the high-pressure metamorphic granitic block (Hu et al., 1993; Shu et al., 1994). A SHRIMP U–Pb zircon age of 968 ± 24 Ma was reported for the high-pressure metamorphic plagiogranite within the serpentinite matrix (Li et al., 1994). In addition, a SHRIMP U–Pb zircon age of 880 ± 19 Ma was determined for a leucogranite, which had been interpreted to be the product of partial melting of sedimentary rocks during the obduction process of the ophiolite (Li et al., 2008). In summary, the ophiolitic mélange was interpreted to constitute fragments of a back-arc basin crust which has formed during convergent tectonics between 1034 and 880 Ma at the margin of the Yangtze plate (Zhao et al., 1995a; Li et al., 1997, 2008) prior to the breakup of Rodinia (Li et al., 2003, 2004). It has also been interpreted as part of Mesozoic overthrust tectonics associated with the collision of the Yangtze and Cathaysian plates (Hsu et al., 1988). However, the hypothesis is still a matter of discussion (e.g. Rowley et al., 1989; Chen et al., 1991). Late Paleozoic radiolaria found in the chert blocks within the serpentinitic matrix (Zhao et al. 1995b; He et al., 1996) and Ar–Ar plateau ages varying between 232 and 266 Ma for plagioclase from the gabbroic blocks (Zhao et al., 1997) support the Mesozoic tectonic origin of the ophiolitic mélange (He et al., 1999; Xiao and He, 2005).

Jadeite, albite and sodic amphibole-bearing meta-granitic blocks have been reported to occur within the Xiwan ultramafic block, which is one of the largest ophiolitic blocks of the NE Jiangxi ophiolitic mélange belt (Fig. 1c and d; Shu and Zhou, 1988; Zhou, 1989). About ten granitic lenses or blocks, the plan view of which varies from 0.5×0.5 m^2 to 1×2 m^2, are exposed within the serpentinite matrix. A sharp, recrystallized contact between the meta-granite and serpentinite is exposed in the field and therefore the meta-granitic blocks are considered to be exotic with regards to the ophiolite mélange, which in turn is enclosed within the Mesoproterozoic Shuangqiaoshan low-grade metamorphic sedimentary strata (Fig. 1d). The adakitic signature of the meta-plagiogranites was first reported by Li and Li (2003). The samples used in the present study were collected from 8 separate granitic blocks from the same area formerly sampled by Li and Li (2003)—(Fig. 1d). A few dark mafic enclaves exposed as darker planar-linear blades (Fig. 2a) or irregular lenses with a plain view varying from 0.5×1 cm^2 to 2×8 cm^2 were observed within weakly-foliated meta-plagiogranite, referred to as (mafic) enclave-bearing meta-plagiogranite or meta-plagiogranite host rock in the following. Similarly meta-plagiogranite without mafic enclaves is called (mafic) enclave-free meta-plagiogranite. The mafic enclave-bearing and -free meta-plagiogranites are exposed as separate blocks and are scattered within the serpentinitic matrix.

3. Petrography of samples

3.1. Mafic enclave-bearing meta-plagiogranite

The host rock of the mafic enclaves (Fig. 2a) is a jadeite-bearing meta-plagiogranite which mainly comprises albite (55%–75%), quartz (11%–33%), clinopyroxene (0.5%–7%), amphibole (3%–14%) and accessory minerals such as rutile, titanite, apatite and zircon (Sample JX153, 154, 158a; Table 1). In general, the mafic enclaves occur as dark elongated lenses with a gradational contact to their host rocks (Fig. 2a). The long axes of the enclaves are parallel to the direction of the darker mineral bands in the host rocks. The meta-plagiogranite host rocks display a porphyroblastic texture which is recrystallized in places. Albite porphyroblasts (1–3 mm) contain jadeite inclusions in the core (Fig. 2b) and are surrounded by fine-grained recrystallized quartz (0.02–0.04 mm). Rutile occurs either as inclusion in albite (Fig. 2c) or as porphyroblastic matrix mineral rimmed by titanite (Fig. 2d). Ilmenite and rutile aggregates are rimmed by titanite (Fig. 2e). Rare monazite and apatite grains occur as inclusions in albite (Fig. 2c). Clinopyroxene occasionally displays an amphibole rim, while titanite and minor apatite occur as matrix minerals (Fig. 2b). Minor anorthite

Fig. 1. (a) Schematic map showing the distribution of the Yangtze and Cathaysian blocks, (b) schematic tectonic map of South China showing the location of the NE Jiangxi ophiolitic mélange belt (modified after Xiao and He, 2005), (c) geological map of the southern segment of the NE Jiangxi ophiolitic mélange belt (modified after He et al., 1999), (d) geological map showing the locality of the high-pressure/low-temperature meta-plagiogranite blocks within the Xiwan serpentinite matrix (modified after Li et al., 2008). 1 = Lower Cretaceous Luotang Formation sandstones; 2 = Lower Cretaceous Shixi Formation volcanics; 3 = Lower Jurassic Linshan Formation sandstones; 4 = Pleistocene sediments; 5 = Holocene sediments; 6 = dip direction and angle; 7 = Lower Cambrian sedimentary rocks; 8 = Lower Sinian Zhitang Formation sedimentary rocks; 9 = Neo-Proterozoic Dengfeng Group sedimentary rocks; 10 = Meso-Proterozoic Shuangqiaoshan Group phyllites and phyllitic siltstones; 11 = Mesozoic granite; 12 = Meso-Proterozoic granodioritic porphyrite; 13 = ophiolitic mélange belt; 14 = serpentinitic block; 15 = unconformity; 16 = fault; 17 = locality of high-pressure/low temperature meta-plagiogranites; 18 = serpentinitic block hosting the high-pressure meta-plagiogranites.

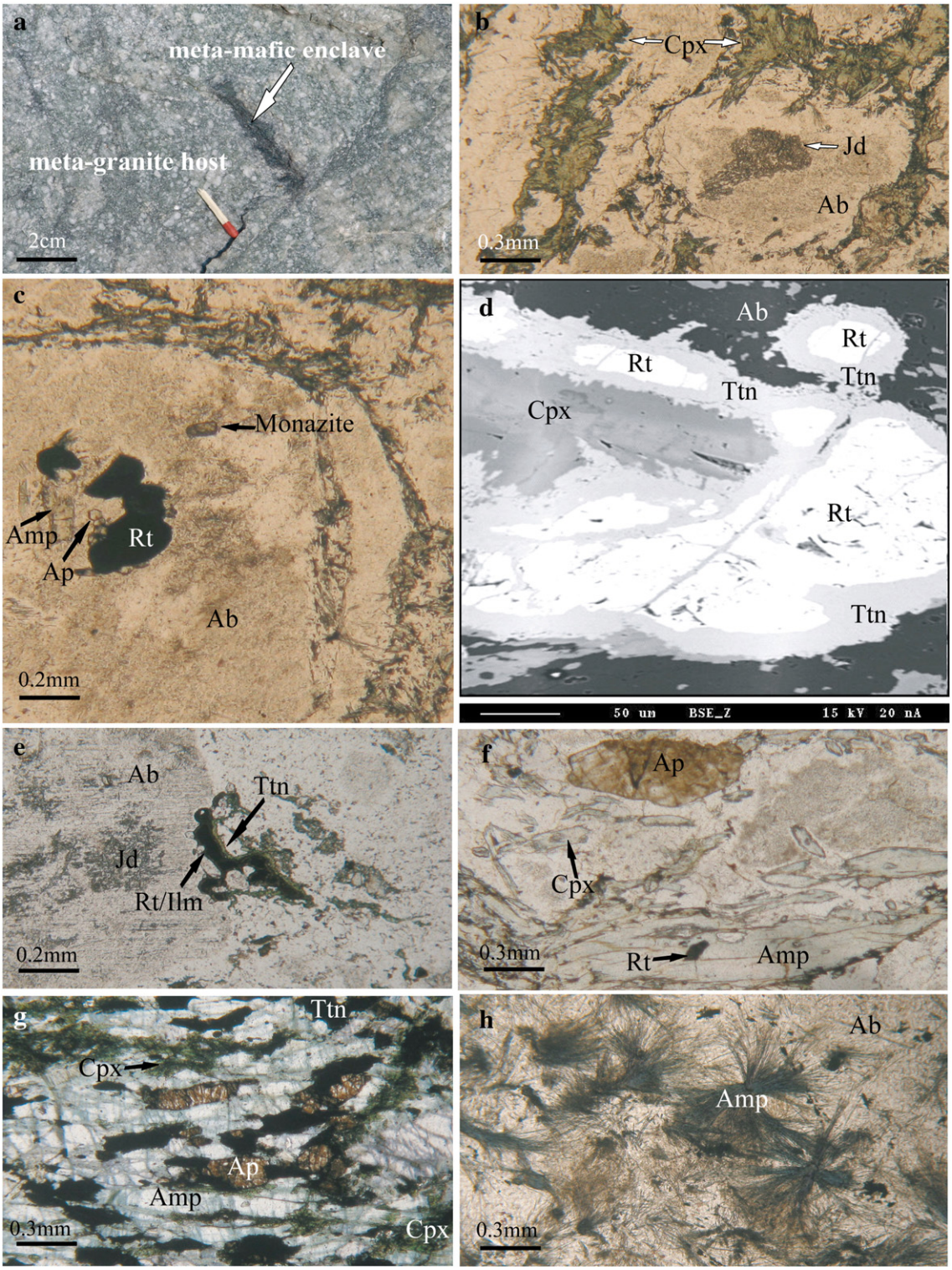

Fig. 2. (a) A meta-mafic enclave in the meta-plagiogranite host rock showing a planar-linear blade shape similar to that of typical 'schlieren' in granites (e.g., Best, 2003), (b) jadeite inclusions in an albite porphyroblast and aegirine augites in the matrix of the meta-plagiogranite host rock (plane-polarized light, sample JX153), (c) rutile, apatite, monazite and amphibole inclusions in an albite porphyroblast (plane-polarized light, sample JX153), (d) back-scattered electronic image showing a rutile grain rimmed by titanite (sample JX153), (e) ilmenite and rutile aggregates in a titanite coexisting with apatite, zircon and aegirine augites (plane-polarized light, sample JX154), (f) winchite grains—with rutile and aegirine augite inclusions—intimately intergrown with apatite (plane-polarized light, sample JX156), (g) the mineral paragenesis of the meta-mafic enclave: aegirine-augite + magnesio-riebeckite + titanite + apatite (plane-polarized light, sample JX158b), (h) radiating magnesio-riebeckite in an enclave-free meta-plagiogranite (plane-polarized light, sample JX182).

and oligoclase was detected in the core of albite by microprobe analyses. Ilmenite and rutile aggregates are rimmed by titanite (Fig. 2e). Minor fine-grained zircons (<0.04 mm) occur as both inclusions in albite and matrix minerals intergrown with quartz. Oriented clinopyroxene and amphibole define weak foliation, which varies in strength in the different blocks. Most albites in the host do not contain relic jadeite inclusions (Sample JX14 and 152; Table 1). The abundances of clinopyroxene and amphibole increase with distance to the mafic enclave and eventually define the foliation of the host meta-plagiogranites. Some oriented blue amphibole porphyroblasts

Table 1
Modal abundances of minerals in the meta-plagiogranite host rock, meta-mafic enclave and enclave-free meta-plagiogranite.

Sample	Rock type	Jd	Cpx	Na-Amp	Amp	Ab	Qtz	Tc	Rt	Ap	Ttn	Ilm	Zr	Mo
JX143	MGH		1.5		3	70	25		<0.2	<0.1	<0.1		<0.1	
JX151	MGH		5.2		13	70	11		<0.5	<0.1	<0.1		<0.1	
JX152	MGH		1.5		3	75	20		<0.3	<0.1			<0.1	
JX153	MGH	1.6	7		1	75	15		<0.1	<0.1	<0.1		<0.1	<0.1
JX154	MGH	0.5	3		1	75	20		<0.1	<0.1	<0.1	<0.1	<0.1	
JX155	MGH		5.6		14	70	10		<0.1	<0.1	<0.1		<0.1	
JX156	MGH		1		10	55	33		<0.3	<0.1	<0.5		<0.1	
JX157	MGH		0.5		10	74	15		<0.1	<0.1	<0.1	<0.1	<0.1	
JX158a	MGH	1.5	5		3	70	20		<0.1	<0.1	<0.1	<0.1	<0.1	
JX158b	MME		5	83	3	3			<0.1	1.5	4.5			
JX182	MG			20		67	10		<0.2	<0.1	2.5	<0.1	<0.1	
JX183	MG			14.5		70	12	<0.1	<0.2	<0.1	3	<0.1	<0.1	

(i) MGH = meta-plagiogranite host; MME = meta-mafic enclave; MG = enclave-free meta-plagiogranite.
(ii) Jd, jadeite; Cpx, clino-pyroxene; Na-Amp, sodic amphibole; Amp, calc-sodic, Fe–Mn–Mg or calcic amphibole; Ab, albite; Qtz, qartz; Rt, rutile; Ttn, titanite; Ilm, ilmenite; Zr, zircon; Tc, talc; Mo, Monazite.

(0.1×0.8 mm^2 to 0.3×1.5 mm^2) contain a few rutile and pyroxene inclusions (Fig. 2 f) and are rimmed by light color actinolite. A few idiomorphic apatites (up to 0.2×0.4 mm^2) are intergrown with blue amphibole, quartz and albite.

3.2. Meta-mafic enclave

Few meta-mafic enclaves are exposed as dark planar-linear blades (Fig. 2a) or irregular lenses. The long axis of enclaves is parallel to or along the foliation of the meta-plagiogranite host rocks. The contact of the mafic-enclaves and the host rocks is either gradational or sheared. These enclaves are predominantly composed of amphibole (86%), clinopyroxene (5%), plagioclase (3%), titanite (4.5%), apatite (1.5%) and minor rutile (Table 1). Oriented amphiboles (0.1×0.5–0.3×1.5 mm^2) define a foliation parallel to the long axes of the enclaves. Clinopyroxene occurs as inclusions in amphibole and as irregular aggregates (Fig. 2g). Elongated titanite grains (0.05×0.2–0.1×0.3 mm^2) and apatite prisms (mainly 0.1×0.3 mm^2) are intergrown with the amphiboles. Rare rutile inclusions could be detected in the core of titanite.

3.3. Mafic enclave-free meta-plagiogranites

This massive rock type mainly consists of amphibole (14.5%–20%), albite (67%–70%), quartz (10%–12%) and accessory minerals such as titanite, rutile, apatite and zircon (Table 1). Amphibole is intergrown with albite porphyroblasts and occasionally occurs as acicular crystals or as radiating aggregates (Fig. 2h). Unorientated albite porphyroblasts (0.3×0.8 mm^2) are surrounded by fine-grained recrystallized quartz. Titanite (up to 3%) is the main accessory mineral. The modal amount of other accessory minerals is less than 0.1 vol.%. Occasionally rare talc booklets are intergrown with amphibole.

4. Analytical method

The major element composition was obtained by X-ray fluorescence analysis (XRF; PHILIPS PW1480) using fused glass disks at the Institute of Mineralogy of the Universität Würzburg. Uncertainties for most major oxides are <2%, for MnO and <5% for P2O5, the totals are within 100 ± 1%. Loss on ignition (LOI) was measured after heating the samples to 1000 °C. Trace element concentrations were analyzed for samples JX143, JX151–157 and JX158, JX181–183 by inductively coupled plasma mass spectrometry (ICP-MS; Finnigan Element) at the Institute of Geology and Geophysics, Chinese Academy of Sciences (IGGCAS) and by a Perkin-Elmer Sciex ELAN 6000 ICP-MS at the Guangzhou Institute of Geochemistry of CAS, respectively. The detailed analytical procedure is described by Qian et al. (2008) and Li and Li (2003). Relative standard deviations (RSD) are within ±10% for most trace elements.

Sr and Nd isotopic compositions were determined on a Finnigan MAT-262 mass spectrometer operated in static mode at the Isotope Laboratory of IGGCAS and the Isotope Laboratory of the Chinese Academy of Geological Sciences (CAGS), respectively. About 100–150 mg of whole rock powder was completely decomposed in a mixture of HF-HClO4. Sr and REE were separated using quartz columns with a 5 ml resin bed of AG 50W-X12, 200–400 mesh. Nd was separated from other REEs by quartz columns using 1.7 ml Teflon® powder as cation exchange medium. Procedural blanks were <200 pg for Sr and <50 pg for Nd. Nd was loaded as phosphates and measured in a Re-double-filament configuration. $^{143}Nd/^{144}Nd$ ratios were normalized to $^{146}Nd/^{144}Nd = 0.7219$ and $^{87}Sr/^{86}Sr$ ratios to $^{86}Sr/^{88}Sr = 0.1194$, respectively.

The major and minor element compositions of silicate minerals and rutile were analyzed on a JEOL JXA 8100 Superprobe at IGGCAS, using an accelerating voltage of 15 kV, beam current of 1×10^{-8} A and spot diameter of 1 μm. Apatite analyses were performed on a Cameca SX50 electron microprobe at the Institute of Mineralogy of the Universität Würzburg. For apatite analyses, the instrument is usually operated with a 10 kV acceleration voltage and a 15 nA beam. Sample spot sizes were *ca.* 10 μm.

The *in situ* trace element contents of the various minerals were measured at the Institute of Mineralogy, Universität Würzburg using a LA-ICP-MS (Agilent 7500i, NewWave LUV 266x). The ablation patterns were single spots (40 μm) with a repetition rate of 5 Hz. For silicates, a laser energy of 0.40 to 0.56 mJ and a laser density of ~44 J/cm^2 were used; for apatites, the laser energy was reduced to 0.13 to 0.3 mJ and a laser density of ~10 J/cm^2 resulting in smaller spots (30 μm) was used. For the apatite measurements, the Ca content of the respective minerals obtained by the electron microprobe acted as the internal standard. For silicates and titanite Si and for rutile Ti were used as internal standards. In order to establish the analytical accuracy analyses of minor elements in all minerals were compared to the respective microprobe results and, in addition, synthetic rutile and titanite (supplied by T. Zack, 2005) were analyzed and used for comparison of trace elements. The calculation of the trace element concentrations was conducted by the GLITTER Version 3.0 on-line interactive data reduction for LA-ICP-MS Program by Macquarie Res. (2000). The 1σ error based on counting statistics from signal and background is <10%.

The SHRIMP (Sensitive High Resolution Ion Microprobe) analyses were performed on the SHRIMP II instrument at the Beijing SHRIMP Center of CAGS. Zircon grains were separated from the crushed rocks by a combined heavy liquid and magnetic separation technique. Individual crystals were mounted in epoxy resin discs together with

Table 2
Representative major element composition of minerals in the meta-plagiogranite host rock, meta-mafic enclave and enclave-free meta-plagiogranite.

Sample	JX153	JX153	JX153	JX153	JX158a	JX158a	JX153	JX153	JX153	JX154	JX154	JX158b	JX158b	JX158b	JX158b
Rock	Meta-plagiogranite host											Meta-mafic enclave			
Location	In albite						In matrix					In matrix			
Mineral	Jd-I	Jd-I	Jd-I	Jd-I	Jd-I	Jd-I	Aug-C	Aug-M	Aug-R	Aug-C	Aug-R	AAug	AAug	AAug	MRie-C
SiO_2	59.51	60.19	59.74	59.70	60.32	60.66	53.37	54.21	54.42	53.95	55.43	53.46	54.42	53.88	58.91
TiO_2	0.00	0.00	0.02	0.02	0.00	0.04	0.54	0.18	0.59	0.36	0.46	0.51	0.16	0.15	0.07
Al_2O_3	24.65	24.68	24.28	24.19	23.76	23.92	2.12	1.89	2.41	0.22	3.57	0.31	0.92	0.28	0.88
Cr_2O_3	0.01	0.00	0.00	0.02	0.00	0.00	0.00	0.00	0.01	0.01	0.03	0.03	0.00	0.00	0.12
FeO*	0.34	0.18	0.36	0.47	1.01	0.93	11.20	9.82	10.29	11.97	9.58	18.63	19.56	17.64	11.16
NiO	0.00	0.00	0.00	0.00	0.04	0.00	0.04	0.07	0.07	0.00	0.03	0.00	0.01	0.01	0.07
MnO	0.00	0.02	0.00	0.00	0.00	0.00	0.09	0.11	0.13	0.16	0.03	0.31	0.19	0.36	0.39
MgO	0.28	0.16	0.35	0.28	0.47	0.28	9.92	11.13	10.12	10.35	9.57	6.29	5.86	7.09	17.89
CaO	0.48	0.27	0.51	0.59	0.92	0.44	17.27	19.68	17.59	19.69	16.12	12.73	10.85	14.94	0.96
Na_2O	15.52	14.67	14.39	15.20	15.14	14.64	4.45	3.37	4.39	2.59	5.20	6.99	8.20	5.64	6.71
K_2O	0.00	0.27	0.40	0.00	0.01	0.05	0.00	0.00	0.02	0.00	0.01	0.03	0.00	0.00	0.07
P_2O_5	n.d.	n.d.	n.d.	n.d.	n.d.	n.d.	n.d.	n.d.	n.d.	n.d.	n.d.	n.d.	n.d.	n.d.	n.d.
Cl	n.d.	n.d.	n.d.	n.d.	n.d.	n.d.	n.d.	n.d.	n.d.	n.d.	n.d.	n.d.	n.d.	n.d.	n.d.
Total	100.79	100.44	100.04	100.46	101.67	100.94	99.00	100.46	100.04	99.29	100.03	99.29	100.16	99.98	97.23
Si	1.99	2.03	2.02	2.01	2.01	2.04	1.98	1.99	2.00	2.03	2.02	2.00	2.01	2.02	8.00
Al	0.97	0.98	0.97	0.96	0.93	0.95	0.09	0.08	0.09	0.01	0.15	0.01	0.04	0.01	0.14
Cr	0.00	0.00	0.00	0.00	0.00	0.00	0.00	0.00	0.00	0.00	0.00	0.00	0.00	0.00	0.01
Ti	0.00	0.00	0.00	0.00	0.00	0.00	0.02	0.01	0.02	0.01	0.01	0.01	0.00	0.00	0.01
Fe^{3+}	0.00	0.00	0.00	0.00	0.00	0.00	0.23	0.17	0.18	0.09	0.15	0.46	0.52	0.36	1.27
Fe^{2+}	0.01	0.01	0.00	0.01	0.03	0.03	0.12	0.13	0.14	0.28	0.15	0.13	0.08	0.20	0.00
Ni	0.00	0.00	0.00	0.00	0.00	0.00	0.00	0.00	0.00	0.00	0.00	0.00	0.00	0.00	n.c.
Mn	0.00	0.00	0.00	0.00	0.00	0.00	0.00	0.00	0.00	0.01	0.00	0.01	0.01	0.01	0.05
Mg	0.00	0.01	0.02	0.01	0.02	0.01	0.55	0.61	0.55	0.58	0.52	0.35	0.32	0.40	3.62
Ca	0.02	0.01	0.02	0.02	0.03	0.02	0.69	0.77	0.69	0.80	0.63	0.51	0.43	0.60	0.14
Na	1.00	0.96	0.95	0.99	0.98	0.96	0.32	0.24	0.31	0.19	0.37	0.51	0.59	0.41	1.77
K	0.00	0.01	0.02	0.00	0.00	0.00	0.00	0.00	0.00	0.00	0.00	0.00	0.00	0.00	0.01
P	n.c.	n.c.	n.c.	n.c.	n.c.	n.c.	n.c.	n.c.	n.c.	n.c.	n.c.	n.c.	n.c.	n.c.	n.c.
Cl	n.c.	n.c.	n.c.	n.c.	n.c.	n.c.	n.c.	n.c.	n.c.	n.c.	n.c.	n.c.	n.c.	n.c.	n.c.
Cation	3.99	4.00	3.99	4.00	4.00	4.00	4.00	4.00	3.99	4.00	4.00	4.00	4.00	4.00	15.01
O	6	6	6	6	6	6	6	6	6	6	6	6	6	6	23
WEF	1.98	1.19	2.38	2.38	2.83	2.83	67.90	75.96	68.89	81.51	63.84	49.60	41.70	59.52	
JD	98.02	98.81	97.62	97.62	95.88	97.17	7.87	6.80	11.24	1.75	18.54	1.48	4.16	1.36	
AE	0.00	0.00	0.00	0.00	0.00	0.00	24.23	17.24	19.87	16.74	17.62	49.92	54.14	39.12	

(i) FeO* as total Fe. (ii) WEF, wollastonite-enstatite-ferrosilite; JD, jadeite; AE, aegirine; Ab, albite; Aug, augite; AAug, aegirine-augite; MRie, magnesio-reibeckite; MFM, Mg–Fe–Mn amphibole; Win, winchite; Act, actinolite;Ap, apatite; Rt, rutile; Ttn, titanite; Ilm, ilmenite; An, anothite; Pl, plagioclase. (iii) I, inclusion mineral; C, the core of mineral; M, the middle of mineral; R, the rim of mineral. (iv) n.d., not determined; n.c., not calculated.

Table 3
Average trace element data of the rock forming minerals of the meta-plagiogranite host rock, meta-mafic enclave and the enclave-free meta-plagiogranite.

Sample	JX153	JX153	JX158b	JX158b	JX158b	JX158b	JX182	JX182	JX156	JX156
Mineral	Jd	Aug	AAug	MFM	MRie	Win	MRie	MRie	Win	Act
Position	Inclusion	In matrix	In matrix	Core	CR	Rim	Core	Rim	Core	Rim
Rock type	MGH	MGH	MME	MME	MME	MME	MG	MG	MGH	MGH
n	4	6	5	1	7	2	1	4	1	1
Sr	805	150	101	92.3	82.5	51.5	58.8	25.8	99.7	127
Y	0.242	2.34	15.7	5.93	7.07	4.92	15.9	12.8	5.89	5.82
Ti	230	7262	9386	4406	8693	974	3413	5097	1995	4128
Nb	0.107	2.53	4.57	2.33	4.58	0.497	13.2	22.3	7.58	9.91
Ta	bdl	bdl	*0.107*	bdl	bdl	bdl	2.39	2.86	0.240	0.244
Zr	1.15	43.9	103	4.22	11.2	7.19	116	137	3.79	5.79
Hf	bdl	1.46	2.54	0.232	0.518	0.368	4.80	7.37	bdl	0.436
La	1.22	5.34	158	2.64	4.94	0.748	12.8	1.08	4.29	1.87
Ce	1.98	8.96	239	4.10	8.02	1.580	36.3	1.76	4.49	2.44
Pr	0.199	0.922	38.3	0.760	1.62	0.202	4.51	*0.243*	0.640	0.418
Nd	0.753	3.52	142	2.56	6.40	0.850	14.8	1.35	1.90	1.92
Sm	bdl	0.619	17.0	0.649	1.58	0.446	3.19	*0.898*	0.651	0.485
Eu	0.179	0.635	3.28	0.279	0.534	*0.102*	0.86	0.288	0.491	0.414
Gd	bdl	bdl	8.46	0.846	1.42	0.910	3.44	1.34	0.946	1.50
Tb	bdl	0.06	0.847	0.134	0.211	0.127	0.684	0.312	bdl	bdl
Dy	bdl	bdl	3.35	1.03	1.36	0.783	4.51	2.69	1.54	1.24
Ho	bdl	bdl	0.455	0.192	0.273	0.154	0.631	0.49	0.297	0.260
Er	bdl	bdl	*1.07*	0.539	0.735	0.673	0.908	1.12	0.964	0.503
Tm	bdl	bdl	0.155	0.087	0.146	0.127	0.116	0.188	0.087	0.116
Yb	bdl	bdl	*1.18*	0.630	1.11	0.779	1.19	1.32	1.23	0.741
Lu	bdl	bdl	0.15	0.116	0.150	0.121	0.230	0.268	bdl	bdl

(i) Pl, plagioclase; Aug, augite; AAug, aegirine-augite; MRie, magnesio-reibeckite; MFM, Mg–Fe–Mn amphibole; Jd, jadeite; Ab, albite; Win, winchite; Act, actinolite; Ap, apatite; Rt, rutile; Ttn, titanite; Ilm, ilmenite. (ii) MGH = meta-plagiogranite host; MME = meta-mafic enclave; MG = enclave-free meta-plagiogranite. (iii) CR = core or rim.

JX158b	JX158b	JX158b	JX158b	JX182	JX182	JX183	JX183	JX156	JX156	JX153	JX153	JX156	JX156	JX158b	JX158b
Meta-mafic enclave				Enclave-free meta-plagiogranite				Meta-plagiogranite host						Mata-enclave	
				In matrix				In matrix		In Act	In Ab	In matrix			
MRie-R	MFM-C	Win-R	Win-R	MRie-C	MRie-R	MRie-C	MRie-R	Win-C	Act-R	MRie-I	Act	Ap	Ap	Ap	Ap
56.15	55.81	56.11	53.13	55.38	55.40	55.15	56.15	57.16	54.44	56.41	55.44	0.10	0.02	0.07	0.11
0.03	0.05	0.30	0.13	0.56	0.57	0.77	1.10	0.03	0.00	0.03	0.05	n.d.	n.d.	n.d.	n.d.
1.19	0.75	0.87	1.72	0.36	0.30	0.87	2.31	0.70	0.16	1.14	1.13	n.d.	n.d.	n.d.	n.d.
0.01	0.02	0.05	0.01	0.05	0.03	0.02	0.01	0.13	0.32	0.03	0.05	n.d.	n.d.	n.d.	n.d.
16.52	18.79	15.53	14.53	24.55	25.10	21.70	20.34	12.35	12.96	8.04	11.42	0.05	0.03	0.15	0.12
0.00	0.03	0.03	0.00	0.00	0.00	0.00	0.02	0.09	0.00	0.02	0.08	n.d.	n.d.	n.d.	n.d.
0.17	0.45	0.17	0.11	0.09	0.12	0.08	0.08	0.26	0.12	0.18	0.18	0.08	0.04	0.07	0.01
13.32	20.27	13.71	14.55	8.27	7.89	9.77	10.23	18.64	15.91	18.79	16.46	0.02	0.93	0.00	0.00
2.03	0.62	5.82	8.93	0.13	0.15	0.08	0.09	3.06	11.52	5.57	12.04	56.33	56.05	55.31	55.17
7.22	0.60	4.62	3.09	7.06	7.11	6.43	6.88	4.30	1.14	5.86	0.83	0.05	0.08	0.09	0.09
0.14	0.01	0.66	0.40	0.04	0.06	0.04	0.04	0.17	0.16	0.18	0.05	n.d.	n.d.	n.d.	n.d.
n.d.	n.d.	n.d.	n.d.	n.d.	n.d.	n.d.	n.d.	n.d.	n.d.	n.d.	n.d.	43.35	42.58	43.06	43.13
n.d.	n.d.	n.d.	n.d.	n.d.	n.d.	n.d.	n.d.	n.d.	n.d.	n.d.	n.d.	0.15	0.21	0.14	0.07
96.79	97.40	97.85	96.60	96.48	96.73	94.90	97.25	96.89	96.74	96.23	97.72	100.12	99.93	98.89	98.69
7.83	7.98	7.93	7.61	8.06	8.07	8.10	7.99	7.93	7.86	7.69	7.88	0.01	0.00	0.01	0.01
0.20	0.13	0.15	0.29	0.06	0.05	0.15	0.39	0.12	0.03	0.18	0.19	n.c.	n.c.	n.c.	n.c.
0.00	0.00	0.01	0.00	0.01	0.00	0.00	0.00	0.01	0.00	0.00	0.01	n.c.	n.c.	n.c.	n.c.
0.00	0.01	0.03	0.01	0.06	0.06	0.09	0.12	0.00	0.00	0.00	0.01	n.c.	n.c.	n.c.	n.c.
1.93	0.06	1.08	1.25	1.67	1.68	1.30	1.29	1.13	0.54	0.92	0.26	n.c.	n.c.	n.c.	n.c.
0.00	2.18	0.76	0.49	1.32	1.37	1.37	1.13	0.31	1.03	0.00	1.10	0.00	0.00	0.01	0.01
n.c.	n.c.	n.c.	n.c.	n.c.	n.c.	n.c.	n.c.	0.00	0.00	0.00	0.00	n.c.	n.c.	n.c.	n.c.
0.02	0.05	0.02	0.01	0.01	0.02	0.01	0.01	0.03	0.02	0.02	0.02	0.01	0.00	0.01	0.00
2.77	4.32	2.89	3.11	1.80	1.71	2.14	2.17	3.86	3.43	3.82	3.49	0.00	0.11	0.00	0.00
0.30	0.10	0.98	1.37	0.02	0.02	0.01	0.01	0.45	1.78	0.82	1.83	4.75	4.75	4.72	4.70
1.95	0.17	1.27	0.86	1.99	2.00	1.83	1.90	1.16	0.32	1.55	0.23	0.01	0.01	0.01	0.01
0.03	0.00	0.12	0.07	0.01	0.01	0.01	0.01	0.03	0.03	0.03	0.01	n.c.	n.c.	n.c.	n.c.
n.c.	n.c.	n.c.	n.c.	n.c.	n.c.	n.c.	n.c.	n.c.	n.c.	n.c.	n.c.	2.89	2.85	2.90	2.91
n.c.	n.c.	n.c.	n.c.	n.c.	n.c.	n.c.	n.c.	n.c.	n.c.	n.c.	n.c.	0.04	0.06	0.04	0.02
15.03	14.99	15.22	15.07	15.01	15.00	15.01	15.01	15.03	15.03	15.03	15.01	7.70	7.78	7.69	7.66
23	23	23	23	23	23	23	23	23	23	23	23	12	12	12	12

(continued on next page)

JX153	JX154	JX156	JX158b	JX153	JX156	JX154	JX158b	JX182	JX154
Ab	Pl	Ap	Ap	Rt	Rt	Ttn	Ttn	Ttn	Ilm
Rim	Core	CR	CR	CR	In matrix	Rim	CR	Core	Core
MGH	MGH	MGH	MME	MGH	MGH	MGH	MME	MG	MGH
2	1	6	6	7	3	1	5	1	2
735	13,590	869	1491	nd	nd	797	900	431	nd
0.092	0.239	257	462	3.41	10.1	21.7	198	269	1.47
41.1	282	779	1358	nd	nd	nd	nd	nd	nd
bdl	0.137	2.13	0.47	2764	4419	169	184	9761	23.2
bdl	0.075	bdl	bdl	89	234	13.9	7.19	618	1.96
1.85	bdl	23.4	4.11	323	466	100	211	877	2.72
bdl	bdl	bdl	bdl	14.1	31.3	4.95	5.98	32.4	bdl
0.77	11.6	240	143	7.68	8.57	16.1	512	597	3.18
1.00	16.3	936	468	6.71	19.6	23.9	447	880	2.36
bdl	1.32	97.4	108	*0.683*	3.74	4.04	153	102	bdl
0.38	4.75	472	574	bdl	bdl	17.5	512	439	bdl
bdl	0.755	112	190	bdl	bdl	5.22	124	100	bdl
0.249	2.82	22.9	28.1	bdl	bdl	4.78	35.7	24.1	bdl
bdl	0.647	116	195	bdl	bdl	6.72	97.4	76.9	bdl
bdl	0.058	11.0	23.9	bdl	bdl	0.993	12.4	20.9	bdl
bdl	bdl	57.0	125	bdl	bdl	2.75	57.7	83.9	bdl
bdl	bdl	9.00	19.6	bdl	bdl	0.767	8.67	13.8	bdl
bdl	bdl	20.4	43.9	bdl	bdl	1.10	20.8	28.0	bdl
bdl	bdl	2.14	5.01	bdl	bdl	*0.21*	2.67	4.22	bdl
bdl	bdl	10.3	24.4	bdl	bdl	1.58	14.6	11.7	bdl
bdl	bdl	1.41	3.08	bdl	bdl	*0.19*	1.75	1.10	bdl

Table 2 (*continued*)

Sample	JX153	JX153	JX153	JX153	JX153	JX153	JX154	JX154	JX154	JX158b	JX158b	JX153	JX153	JX154
Rock	Meta-plagiogranite host									Mata-enclave		Meta-plagiogranite host		
Location	In matrix									In Ttn	In matrix	In Ab	Rim	In Ab
Mineral	Rt-C	Rt-M	Ttn-R	Ilm-C	Rt-M	Ttn-R	Ilm-C	Rt-M	Ttn-R	Rt-I	Ttn-R	An-I	Ab-R	Pl-I
SiO_2	0.09	0.30	30.85	0.02	0.12	25.24	0.02	0.17	30.88	0.57	31.22	45.10	67.70	59.77
TiO_2	98.44	98.99	40.72	51.29	98.45	50.59	54.05	96.02	39.11	96.19	38.09	0.03	0.00	0.00
Al_2O_3	0.00	0.02	0.12	0.00	0.02	0.47	0.05	0.00	0.12	0.00	0.80	31.58	20.06	24.04
Cr_2O_3	0.16	0.16	0.04	0.01	0.42	0.10	0.00	0.30	0.18	0.01	0.10	0.02	0.00	0.00
FeO*	0.13	0.13	0.01	46.93	0.85	0.19	43.67	0.37	0.39	0.15	0.42	0.94	0.05	0.20
NiO	0.00	0.03	0.00	0.00	0.00	0.06	0.00	0.00	0.00	0.00	0.01	0.05	0.00	0.00
MnO	0.00	0.00	0.00	1.69	0.00	0.04	1.67	0.00	0.01	0.01	0.01	0.00	0.00	0.00
MgO	0.00	0.00	0.00	0.21	0.00	0.00	0.00	0.00	0.00	0.00	0.00	0.00	0.22	0.92
CaO	0.38	0.83	28.14	0.40	0.80	23.39	0.00	0.81	27.89	1.38	27.57	19.98	0.03	7.30
Na_2O	0.03	0.03	0.21	0.00	0.03	0.00	0.00	0.01	0.11	0.00	0.10	2.27	11.71	7.96
K_2O	0.01	0.00	0.01	0.00	0.02	0.02	0.00	0.00	0.01	0.01	0.04	0.05	0.03	0.06
P_2O_5	n.d.	n.d.	n.d.	n.d.	n.d.	n.d.	n.d.	n.d.	n.d.	n.d.	n.d.	n.d.	n.d.	n.d.
Cl	n.d.	n.d.	n.d.	n.d.	n.d.	n.d.	n.d.	n.d.	n.d.	n.d.	n.d.	n.d.	n.d.	n.d.
Total	99.23	100.49	100.1	100.6	100.70	100.08	99.46	97.69	98.67	98.33	98.35	100.00	99.80	100.262
Si	0.00	0.00	1.00	0.00	0.00	0.83	0.00	0.00	1.02	0.01	1.03	2.12	2.97	2.67
Al	0.00	0.00	0.00	0.00	0.00	0.02	0.00	0.00	0.00	0.00	0.03	1.74	1.04	1.26
Cr	0.00	0.00	0.00	0.00	0.00	0.00	0.00	0.00	0.01	0.00	0.00	0.00	0.00	0.00
Ti	0.99	0.99	1.00	0.98	0.98	1.25	1.02	0.99	0.97	0.98	0.97	0.00	0.00	0.00
Fe^{3+}	0.00	0.00	0.00	0.00	0.00	0.00	0.00	0.00	0.00	0.00	0.00	0.00	0.00	0.00
Fe^{2+}	0.00	0.00	0.00	0.99	0.01	0.01	0.92	0.00	0.01	0.00	0.01	0.04	0.00	0.01
Ni	0.00	0.00	0.00	0.00	0.00	0.00	0.00	0.00	0.00	0.00	0.00	0.00	0.00	0.00
Mn	0.00	0.00	0.00	0.04	0.00	0.00	0.04	0.00	0.00	0.00	0.00	0.00	0.00	0.00
Mg	0.00	0.00	0.00	0.01	0.00	0.00	0.00	0.00	0.00	0.00	0.00	0.00	0.01	0.06
Ca	0.01	0.01	0.98	0.01	0.01	0.82	0.00	0.01	0.99	0.02	0.98	1.00	0.00	0.35
Na	0.00	0.00	0.01	0.00	0.00	0.00	0.00	0.00	0.01	0.00	0.01	0.21	1.00	0.69
K	0.00	0.00	0.00	0.00	0.00	0.00	0.00	0.00	0.00	0.00	0.00	0.00	0.00	0.00
P	n.c.	n.c.	n.c.	n.c.	n.c.	n.c.	n.c.	n.c.	n.c.	n.c.	n.c.	n.c.	n.c.	n.c.
Cl	n.c.	n.c.	n.c.	n.c.	n.c.	n.c.	n.c.	n.c.	n.c.	n.c.	n.c.	n.c.	n.c.	n.c.
Cation	1.00	1.00	3.00	2.03	1.01	2.92	1.98	1.00	3.01	1.01	3.04	5.11	5.02	5.04
O	2	2	5	3	2	5	3	2	5	2	5	8	8	8
WEF														
JD														
AE														

pieces of the Canberra standard TEMORA (417 Ma; Black et al., 2003). The discs were polished and zircons were half sectioned, followed by cleaning and gold-coating. Cathodoluminescence (CL) images were taken by the Hitachi S-3000N Scanning Electron Microscope at CAGS. Spot sizes for the SHRIMP analyses averaged 30 μm and mass resolution was at about 5000 for the measurements of the Pb/Pb and Pb/U isotopic ratios. The ^{238}U concentrations were normalized to the standard SL13 ($^{238}U = 238$ ppm; age: 572 Ma). The analyses of standard TEMORA and samples were alternated (1:3) for correcting Pb^+/U^+ discrimination. The data reported in this study were corrected by assuming $^{206}Pb/^{238}U$–$^{208}Pb/^{232}Th$ age-concordance. The SQUID (Version 1.03d) and ISOPLOT (Version 3.00) programs of K.R. Ludwig (1991) were used to process the data.

5. Results

5.1. Mineral chemistry

The representative major and trace element composition of minerals which are presented in Table 2 and Table 3, respectively, were obtained from three enclave-free meta-plagiogranites, two enclave-bearing meta-plagiogranites and one meta-mafic enclave.

5.1.1. Clinopyroxene group

Jadeite inclusions in albite porphyroblasts of enclave-bearing meta-plagiogranite have high jadeite (>97 mol%) and minor WEF components (wollastonite–enstatite–ferrosilite; cf. Morimoto, 1988; Fig. 3). Matrix clinopyroxene is classified as aegirine augite to augite with an average WEF component of 75.4 mol%, jadeite component of 6 mol% and aegirine component of 18.6 mol%. The clinopyroxene of the meta-mafic enclave is classified as aegirine augite (Fig. 3) with an average aegirine component of 43.5 mol%, WEF of 51.4 mol% and jadeite of 5.1 mol%. Jadeite contains 805 ppm Sr and 230 ppm Ti while the concentration of other trace elements is less than 2 ppm. The

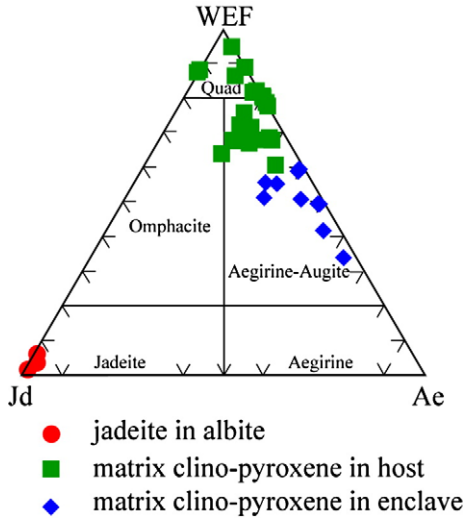

Fig. 3. Composition of clinopyroxene in the meta-plagiogranite host rocks and the meta-mafic enclave.

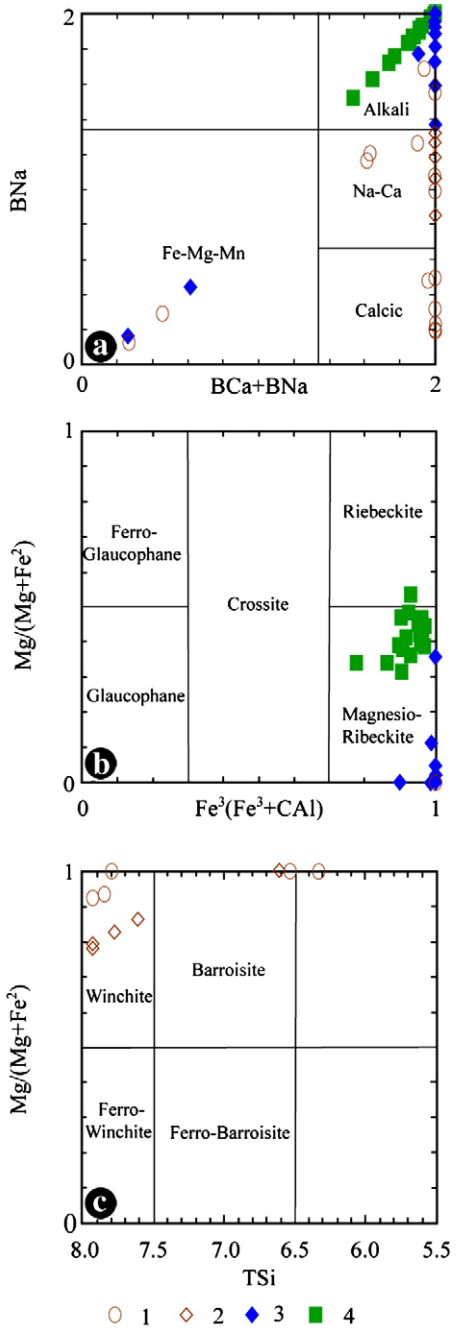

Fig. 4. Composition of amphiboles in the meta-plagiogranite host rocks, the meta-mafic enclave and the enclave-free meta-plagiogranites. (a) Classification for alkali, sodic-calcic, calcic and Fe–Mg–Mn groups, (b) classification for alkali amphiboles, (c) classification for sodic-calcic amphiboles. 1—amphibole rims in the matrix of meta-plagiogranite host rocks, 2—amphibole rims in the meta-mafic enclave, 3—amphibole cores in the meta-mafic enclave, 4—amphiboles in the matrix of enclave-free meta-plagiogranites.

aegirine augite of the meta-mafic enclave displays a higher trace element concentration than the matrix clinopyroxene of the meta-plagiogranite host rocks (relative average compositions are 9386 ppm vs. 7262 ppm Ti, 15.7 ppm vs. 2.34 ppm Y, 103 ppm vs. 43.9 ppm Zr, 158 ppm vs. 5.34 ppm La, 3.28 ppm vs. 0.635 ppm Eu, 1.18 ppm vs. below detection limit Yb).

5.1.2. Amphibole group

The compositional range of the amphiboles includes sodic, sodic-calcic, calcic and Mg–Fe–Mn groups on the basis of Leake's (1997) classification (Fig. 4a). Sodic amphiboles predominantly occur as matrix minerals in the meta-mafic enclave and the enclave-free meta-plagiogranites. Occasionally, it occurs as inclusions in the core of aegirine–augite in the enclave-bearing meta-plagiogranites. The sodic amphibole is magnesio-riebeckite in the mafic enclave (Fig. 4b) while that in the enclave-free meta-plagiogranites has a lower sodic content and $Fe^{3+}/Fe^{3+}+Al^{VI}$ ratio and a higher $Mg/Mg+Fe^{2+}$ ratio. Sodic-calcic amphibole occurs as the rims of magnesio-riebeckite in the meta-mafic enclave and aegirine-augite in the meta-plagiogranite host rocks. Na_2O ranges from 3.09 wt.% to 4.84 wt.%, displaying a winchite or barroisitic composition (Fig. 4c). The calcic amphibole has an actinolitic composition and also occurs as the rims of magnesio-riebeckite and aegirine-augite. Na_2O of actinolites ranges from 0.72 wt.% to 1.82 wt.%, CaO from 10.77 wt.% to 12.04 wt.%. Mg–Fe–Mn amphibole is rare and predominantly occurs as inclusions in the core of magnesio-riebeckite in the meta-mafic enclave and in albite and aegirine-augite cores in the enclave-bearing meta-plagiogranites. It is classified as anthophyllite, magnesio-cummingtonite or cummingtonite-anthophyllite with an average composition of 1.09 wt.% Na_2O, 1.02 wt.% CaO, 1.35 wt.% Al_2O_3, 20.24 wt.% MgO, 17.58 wt.% FeO, and 0.66 wt.% MnO. Magnesio-riebeckite in enclave-free meta-plagiogranites has relatively lower concentrations of LREEs and higher concentrations of HREEs compared with the magnesio-riebeckite in the meta-mafic enclave and the sodic-calcic amphiboles in meta-plagiogranite host rocks (Fig. 5a; Table 3). Concentrations of Ti, Nb, Ta, Zr and Hf increase while LREEs and Y decrease from core to rim. Moreover, the average composition of Ti increases from 3413 to

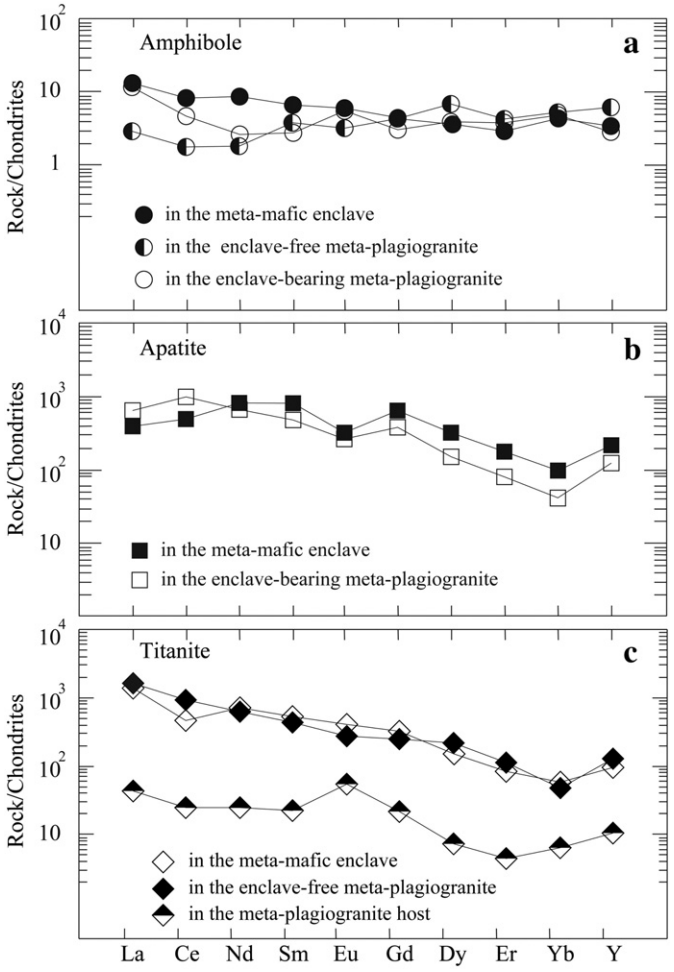

Fig. 5. Chondrite-normalized REE diagrams for amphibole (a), apatite (b) and titanite (c) of the meta-plagiogranite host rocks, the meta-mafic enclave and the enclave-free meta-plagiogranites. Normalization values are after Taylor and McLennan (1985).

5097 ppm, Nb from 13.2 to 22.3 ppm, Zr from 116 to 137 ppm, whereas La decreases from 12.8 to 1.08, Eu from 0.850 to 0.288 ppm and Y from 15.9 to 12.8 ppm from core to rim (Table 3). The trace element contents of actinolite and Mg–Fe–Mn amphibole are relatively low, with REE below 1 ppm, Y below 6 ppm, Nb below 10 ppm and Zr below 6 ppm.

5.1.3. Plagioclase group

Albite occurs as porphyroblasts in the meta-plagiogranite host rock and enclave-free meta-plagiogranite. Compositional inhomogeneities of the albite porphyroblasts are displayed by rare anorthite-rich plagioclase (An > 80 vol.%) inclusions, which were detected during microprobe analyses in the albite core. Thus the original igneous plagioclase probably had a higher An content which was lost during recrystallization under LT–HP metamorphism. Apart from Sr, Ti, La and Eu, the concentration of most trace elements is very low, usually below the detection limit. Plagioclase with a high An content displays much higher Sr and Eu concentrations than pure albite (13,590 ppm vs. 735 ppm Sr, 2.82 ppm vs. 0.249 ppm Eu; Table 3).

Apatite in the meta-plagiogranite host rocks has similar CaO and P_2O_5 contents to that in the meta-mafic enclave; the former has an average CaO content of 56.2 wt.% and P_2O_5 of 42.9 wt.%, whereas the

Table 4
Major, trace element and Sr-Nd isotopic compositions of the meta-plagiogranite host rock, meta-mafic enclave and enclave-free meta-plagiogranite.

Sample	JX143	JX151	JX152	JX153	JX154	JX155	JX156	JX157	JX158b	JX181	JX182	JX183
Rock type	Meta-plagiogranite host								Meta-mafic enclave	Enclave-free meta-plagiogranite		
SiO_2	70.87	65.03	70.69	69.39	69.23	67.28	72.33	67.22	52.14	67.89	65.25	69.96
TiO_2	0.24	0.54	0.34	0.23	0.23	0.20	0.20	0.24	4.63	0.38	0.28	0.28
Al_2O_3	15.09	16.74	14.65	16.28	15.81	16.53	14.38	17.43	5.94	16.27	16.23	15.73
Fe_2O_3T	1.78	2.81	1.93	1.63	2.17	2.61	1.63	1.87	13.12	3.98	3.70	2.30
MnO	0.01	0.03	0.02	0.01	0.02	0.02	0.02	0.02	0.22	0.02	0.02	0.01
MgO	1.30	1.15	0.89	0.80	0.94	1.50	1.26	0.75	8.45	1.44	2.94	0.97
CaO	1.16	2.92	2.10	1.57	1.76	1.99	1.64	2.05	5.34	0.40	0.23	0.27
Na_2O	8.44	9.62	8.16	8.79	8.87	8.67	7.39	8.97	6.52	7.24	10.08	9.32
K_2O	0.28	0.30	0.25	0.45	0.39	0.52	0.35	0.64	0.57	0.89	0.10	0.10
P_2O_5	0.06	0.13	0.16	0.06	0.06	0.06	0.06	0.07	1.21	0.15	0.08	0.11
LOI	0.25	0.14	0.10	0.19	0.10	0.26	0.33	0.39	0.95	1.08	0.38	0.12
Total	99.48	99.41	99.29	99.40	99.58	99.64	99.59	99.65	99.09	99.74	99.29	99.17
A/CNK	0.93	0.78	0.84	0.91	0.87	0.90	0.93	0.91		1.20	0.95	0.99
Mg#	61.9	47.7	50.7	52.2	49.1	56.1	63.3	47.2	58.9	44.6	63.9	48.4
Be	0.813	0.738	0.832	0.81	0.837	0.766	0.7869	0.834	0.987	1.15	1.66	1.09
Sc	2.2	2.4	0.7	0.6	1.42	0.779	1.08	1.42	17.9	2.49	1.88	1.48
V	13.1	33.9	14.8	11	10.9	14.4	6.5	38	208	23.0	23.6	13.2
Cr	24.1	7.94	23.3	17.7	25.6	42.1	21.3	12.5	78.8	2.60	6.50	14.20
Co	4.72	4.68	3.69	3.14	4.2	6.08	4.78	5.27	40.9	4.39	2.77	4.30
Ni	29.5	24.4	17	77.7	35.2	34.4	36.3	33.6	181	1.76	10.5	17.3
Ga	18	16.3	14.7	15.4	17	18.8	15.4	18.3	10.1	16.3	17.3	14.3
Rb	2.77	3.46	2.13	3.22	2.81	4.20	2.80	5.23	1.98	25.2	3.45	2.42
Sr	272	570	308	728	526	511	429	535	363	417	123	255
Cs	0.169	0.224	0.046	0.51	0.253	0.081	0.192	0.228	0.126	1.41	0.202	0.064
Ba	412	103	62.1	144	124	89.9	85.0	137	40.2	322	94.8	176
Y	2.6	3.71	3.21	2.02	1.71	1.23	1.77	2.35	24.4	13.4	12.6	13.0
Nb	1.24	4.49	2.85	2.42	2.41	1.48	13.7	2.33	19.0	19.5	21.6	18.7
Ta	0.189	0.518	0.204	0.2	0.247	0.157	0.946	0.194	0.62	1.31	1.67	1.24
Zr	102	107	74.2	69.2	52.4	65.7	70.9	81.0	697	188	198	176
Hf	3.02	2.44	2.11	1.96	1.50	1.92	2.19	2.36	15.9	4.52	5.06	4.57
Pb	1.31	7.86	0.372	1.89	1.39	0.793	0.756	2.28	4.32	4.99	6.36	3.23
Th	1.6	0.709	0.736	1.24	0.936	1	2.13	1.88	1.03	7.01	9.31	11.0
U	0.227	0.382	0.199	0.19	0.145	0.131	0.222	0.222	1.04	1.75	2.24	2.50
La	10.6	6.31	6.62	9.35	6.67	8.42	16.7	12.2	14.4	34.4	40.8	41.5
Ce	21.1	12.4	12.6	14.7	12.1	13.7	28.3	21.1	37.4	66.0	72.9	72.5
Pr	2.51	1.52	1.69	1.93	1.44	1.77	3.28	2.56	6.40	7.45	8.38	8.18
Nd	9.40	6.00	6.93	7.44	5.12	6.78	10.3	8.84	33.1	26.3	26.3	25.6
Sm	1.62	1.47	1.45	1.12	0.866	0.929	1.34	1.39	9.48	4.17	3.94	4.01
Eu	0.488	0.550	0.603	0.468	0.420	0.343	0.499	0.608	1.64	1.08	1.04	1.28
Gd	1.30	1.22	1.31	0.924	0.794	0.696	1.13	1.11	7.73	3.01	2.98	3.21
Tb	0.152	0.151	0.171	0.112	0.097	0.082	0.115	0.132	1.13	0.447	0.410	0.445
Dy	0.624	0.751	0.780	0.429	0.376	0.304	0.428	0.520	5.04	2.28	2.27	2.37
Ho	0.103	0.134	0.138	0.081	0.075	0.055	0.072	0.098	0.852	0.422	0.418	0.459
Er	0.261	0.352	0.325	0.205	0.185	0.151	0.196	0.247	2.15	1.21	1.18	1.26
Tm	0.041	0.054	0.049	0.029	0.026	0.020	0.026	0.035	0.272	0.180	0.179	0.195
Yb	0.238	0.352	0.270	0.172	0.147	0.115	0.169	0.218	1.95	1.33	1.33	1.34
Lu	0.031	0.051	0.039	0.027	0.023	0.018	0.027	0.034	0.316	0.219	0.219	0.213
∑REE	48.457	31.27	33.000	36.940	28.362	33.407	62.532	49.099	121.858	148.434	162.336	162.494
Eu/Eu*	1.03	1.26	1.34	1.40	1.55	1.30	1.24	1.49	0.59	0.93	0.92	1.09
Sr/Y	105	154	96.0	360	308	415	242	228	15	31	10	20
(La/Yb)N	30	12	17	37	31	49	67	38	5	17	21	21
$^{87}Rb/^{86}Sr$				0.0128	0.0154	0.0238	0.0190		0.0158	0.1748		0.0247
$(^{87}Sr/^{86}Sr)m$				0.702892	0.702896	0.702907	0.702847		0.702534	0.706159		0.704908
2σ error				0.000018	0.000018	0.000020	0.000020		0.000012	0.000012		0.000014
$(^{87}Sr/^{86}Sr)i$				0.7027	0.7027	0.7026	0.7026		0.7023	0.7037		0.7045
$^{147}Sm/^{144}Nd$				0.09128	0.10230	0.08284	0.07930		0.17340	0.09590		0.09490
$^{143}Nd/^{144}Nd$				0.512344	0.512377	0.512270	0.512248		0.512807	0.511931		0.511928
2σ error				0.000008	0.000009	0.000007	0.000008		0.000007	0.000010		0.000012
εNd(970 Ma)				7.37	6.64	6.97	6.98		6.2	−1.28		−1.22

(i) Total iron as Fe_2O_3; (ii) Mg# = Mg/(Mg + Fe^{2+}), assuming FeO/Fe_2O_3T=0.80; (iii) A/CNK = molar ratio of Al_2O_3/(CaO + Na_2O + K_2O).

latter has 55. 2 wt.% and 42.9 wt.%, respectively. The Cl content of apatite is very low (<0.21 wt.%). However, apatite contains high concentrations of almost all trace elements except Nb, Ta, Zr and Hf (Table 3; Fig. 5b). Apatite in the meta-mafic enclave has lower concentrations of La and Ce and higher concentrations of all other REE and Y than that in the meta-plagiogranite host rocks, i.e. 143 vs. 240 ppm La, 468 vs. 936 ppm Ce, 108 vs. 97.4 ppm Pr, 574 vs. 472 ppm Nd, 24.4 vs. 10.3 ppm Yb, and 462 vs. 257 ppm Y.

5.1.4. Rutile, titanite and ilmenite

Trace element concentrations of rutile inclusions in titanite were not determined due to their small grain size. Rutile in meta-plagiogranite host rocks contains high concentrations of high field strength elements (HFSE) such as Nb, Ta, Zr, Hf and LREEs such as La, Ce and Pr. However, the concentrations of all other REEs are below the detection limit. Two rutiles in samples JX153 and JX156 have Nb = 2764 and 4419 ppm, Ta = 89 and 234 ppm, Zr = 323 and 466 ppm and Hf = 14.1 and 31.3 ppm, respectively.

Titanite in the meta-mafic enclave has higher SiO_2 and Al_2O_3 contents and lower TiO_2 contents than that in the meta-plagiogranite host rocks (e.g., 31.22 vs. 30.83 wt.% SiO_2, 0.80 vs. 0.12 wt.% Al_2O_3, and 38.09 vs. 40.72 wt.% TiO_2). It contains high concentrations of both HFSE and REE (Table 3; Fig. 5c). Titanite in the meta-mafic enclave has much higher concentrations of REEs and Y than that in the meta-plagiogranite host rocks (Fig. 5c); e.g., 512 vs. 16.1 ppm La, 447 vs. 23.9 ppm Ce, 14.6 vs. 1.58 ppm Yb, and 198 vs. 21.7 ppm Y. The REE and Y concentrations of titanite in enclave-free meta-plagiogranites are similar to those in the meta-mafic enclave, but the former has much higher Nb (9761 vs. 184 ppm), Ta (618 vs. 7.2 ppm), Zr (877vs. 211 ppm) and Hf (32.4 vs. 6 ppm) concentrations.

Ilmenite has an average composition of 49.1 wt.% TiO_2, 47.7 wt.% FeO and 1.5 wt.% MnO. Apart from minor Nb (23.2 ppm), Ta (1.96 ppm) and Zr (2.72 ppm), no other trace elements were detected.

5.2. Whole rock chemistry

Major and trace elements and Sr–Nd isotopic compositions are presented in Table 4. The mafic enclave-bearing meta-plagiogranites have an average SiO_2 content of 69 wt.% and are granites based on the classification of Middlemost (1994), or trondhjemites and albite granites according to Li and Li (2003). Al_2O_3 ranges from 14.38 to 17.43 wt.%, Na_2O from 7.39 to 9.62 wt.%, K_2O from 0.28 to 0.52 wt.%, TiO_2 from 0.20 to 0.54 wt.% and Mg# from 47.7 to 63.3. They are metaluminous with A/CNK values varying from 0.78 to 0.93. In general, Al_2O_3 and Na_2O decrease with increasing SiO_2 (Fig. 6). They display a strongly REE fractionated pattern (Fig. 7a), with a slight LREE-enrichment, strong HREE-depletion and positive Eu anomalies. Their $(La/Yb)_N$ ranges from 12 to 67, $(Gd/Yb)_N$ from 2.8 to 5.4 and Eu/Eu* from 1.03 to 1.55. The Yb (0.216 ppm) and Y (2.33 ppm) concentrations of the enclave-bearing meta-plagiogranites are lower than those of chondrite and primitive mantle, respectively (Taylor and McLennan, 1985), and thus are significantly depleted in HREE and Y in the primitive normalized spidergram (Fig. 7b). These rocks display a strong Sr anomaly and are weakly depleted in Nb and Ta. Their Sr concentration varies between 272 and 728 ppm. The Sr and Ba concentrations display no linear trend with increasing SiO_2 (Fig. 6).

The mafic enclave has a basaltic composition with SiO_2 = 52 wt.%, Na_2O = 6.52 wt.%, TiO_2 = 4.63 wt.%, and P_2O_5 = 1.21 wt.%. It displays a flat REE distribution pattern with a negative Eu anomaly (Eu/Eu* = 0.59; Fig. 7a). The HREE and Y concentrations are about 10

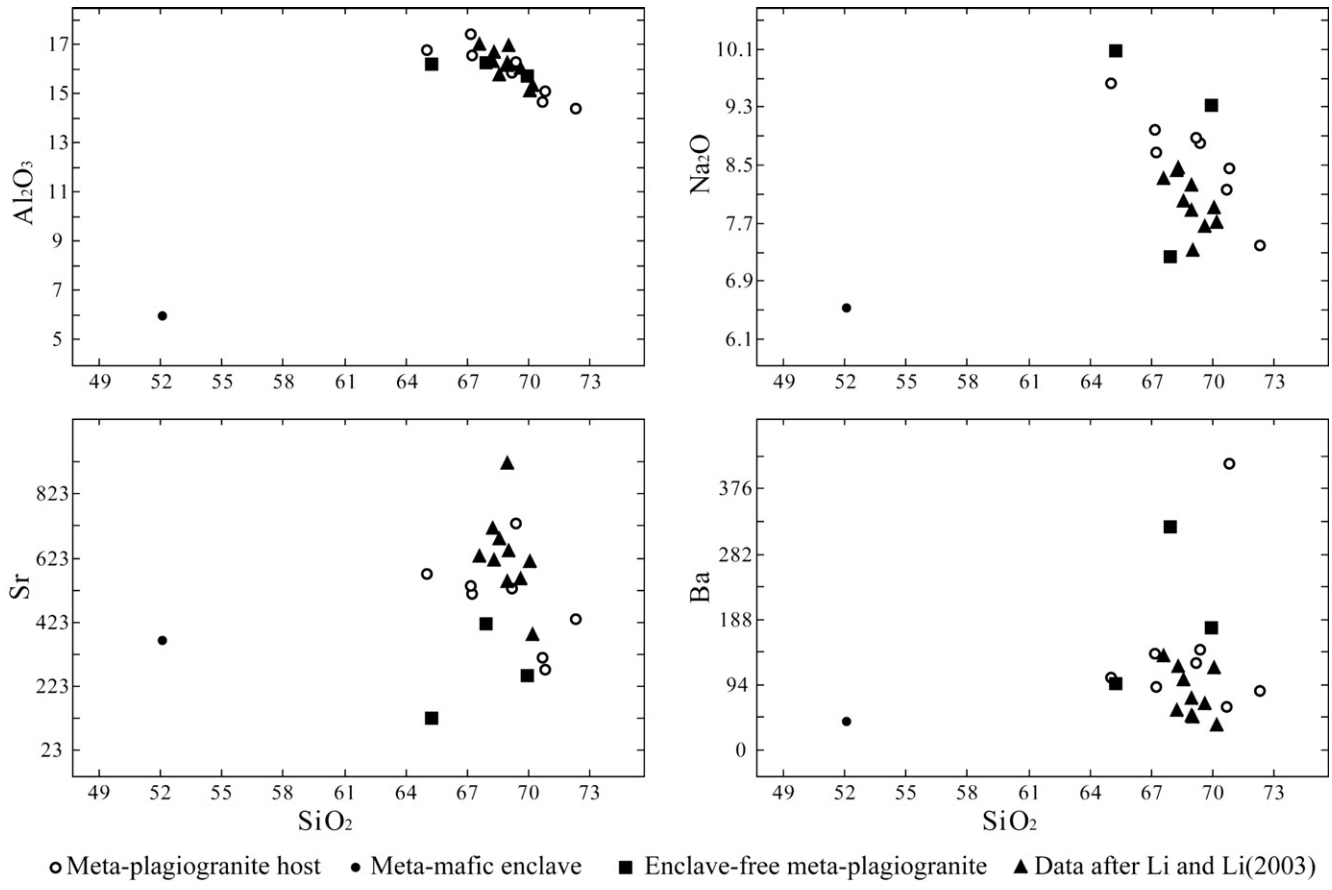

Fig. 6. Harker-type chemical variation diagrams for the meta-plagiogranite host rocks, the meta-mafic enclave and the enclave-free meta-plagiogranites.

times higher relative to those of the host meta-plagiogranites. In the primitive-normalized spidergram, it displays a slight depletion in Sr and Eu and a slight enrichment in Nb and Zr (Fig. 7c).

The enclave-free meta-plagiogranite is weakly metaluminous with an A/CNK = 0.97 or weakly peraluminous with an A/CNK = 1.2. It is also characterized by high Al_2O_3 (16.08 wt.%), Na_2O (8.88 wt.%) and Mg# (52.3), and low K_2O (0.36 wt.%) and TiO_2 (0.31 wt.%). It further displays a slight enrichment of LREE with (La/Yb)N = 20.2. Eu/Eu* ranges from 0.92 to 1.09. In the primitive mantle-normalized spidergram, this rock type displays a slight depletion in Sr and Nb (Fig. 7c). The Y and Yb concentrations (average 20 and 1.33 ppm, respectively) are much higher than those of the enclave-bearing meta-plagiogranite and lower than those of the mafic enclave.

The mafic enclave-bearing meta-plagiogranite has a $^{87}Sr/^{86}Sr$ value of 0.7026 to 0.7027 and a high $\varepsilon Nd(T)$ of 6.6 to 7.4, similar to those of MORBs (Fig. 8). An age of 970 Ma is chosen for the calculation

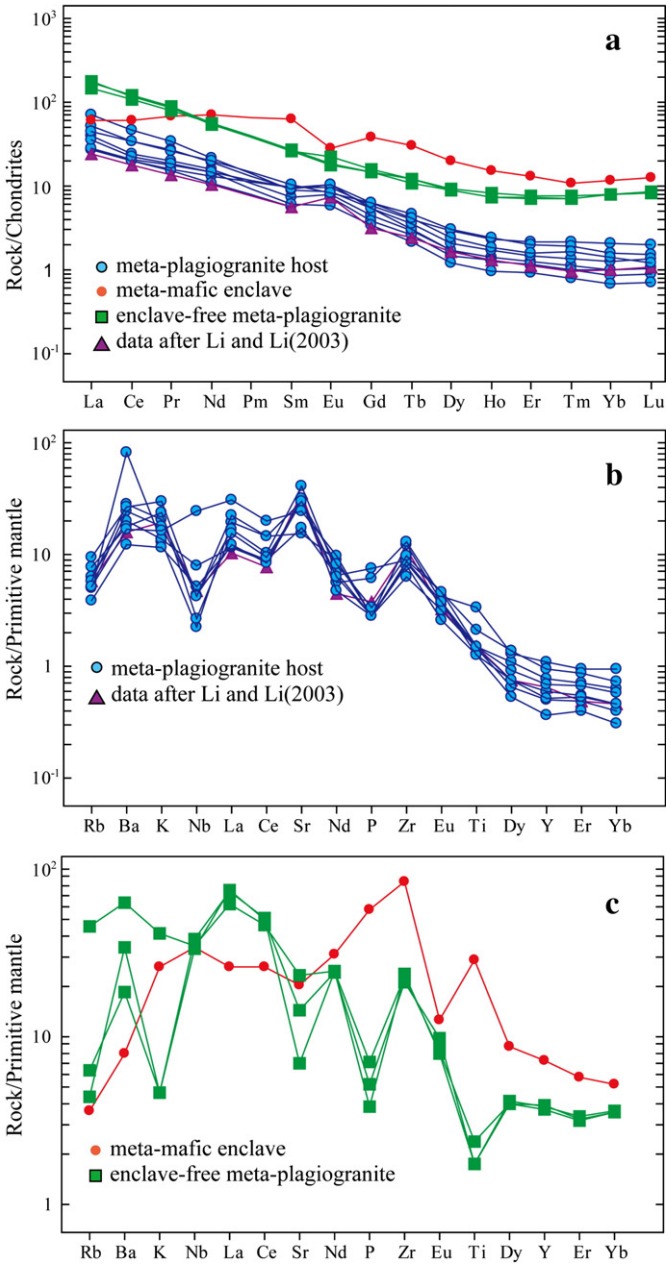

Fig. 7. (a) Chondrite-normalized REE diagrams and (b) primitive mantle-normalized spidergrams for the meta-plagiogranite host rocks, the meta-mafic enclave and the enclave-free meta-plagiogranites. Normalization values are after Taylor and McLennan (1985).

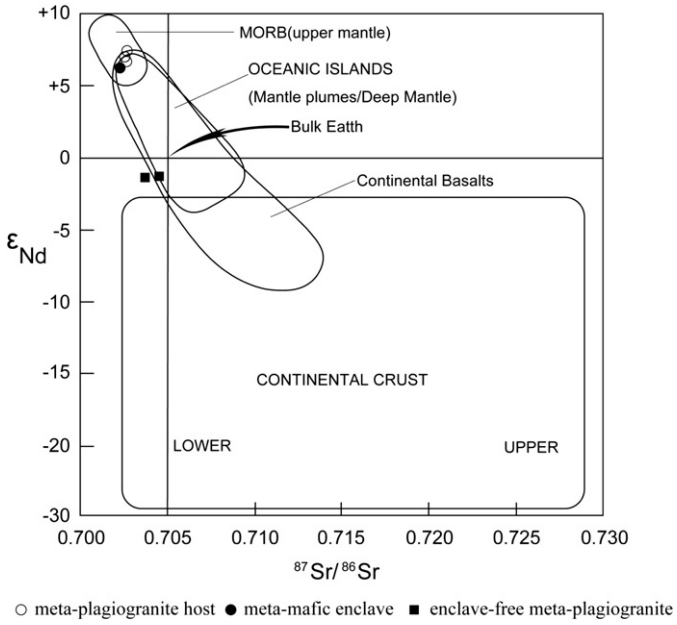

Fig. 8. Sr vs. Nd isotope ratio plots of the meta-plagiogranite host rocks, the meta-mafic enclave and the enclave-free meta-plagiogranites. The Sr and Nd isotope ratios of geochemical reservoirs are after White (2007).

on the basis of the SHRIMP zircon U–Pb ages obtained in this study and by Li et al. (1994). The initial Sr and Nd values of the meta-mafic enclave are similar to those of its host meta-plagiogranites ($^{87}Sr/^{86}Sr = 0.7023$ and $\varepsilon Nd(T) = 6.2$; (Fig. 8)). The mafic enclave-free meta-plagiogranite has $^{87}Sr/^{86}Sr$ ratios between 0.7037 and 0.7045 and an $\varepsilon Nd(T)$ between −1.22 and −1.28 (Fig. 8).

5.3. SHRIMP age dating results for zircons

U–Pb analyses were conducted by the SHRIMP method on zircon grains separated from one enclave-bearing meta-plagiogranite sample (Sample JX154). The results are presented in Table 5. Zircon grains are usually either elongated or display short prisms and range in size from 100 to 500 μm. They are colorless to light brown, transparent and euhedral with well-developed concentric oscillatory zoning, indicating a magmatic origin (Fig. 9a). Among 15 spots analyzed, eight concordant points give a weighted mean $^{206}Pb/^{238}U$ age of 970 ± 21 Ma (Fig. 9b). Other discordant points were not considered since they were interpreted to reflect to the disturbance of the U–Pb isotopic system i.e. multiple Pb loss during later-stage deformational events which may account for the younger ages (Li et al., 1994). The result corresponds well with the 968 ± 23 Ma age previously obtained by Li et al. (1994).

6. Discussion

6.1. Metamorphic processes and primary magmatic mineral paragenesis of high-pressure rocks

The mineral assemblages and textures of the meta-plagiogranite host rock, the meta-mafic enclave and the mafic enclave-free meta-plagiogranite have undergone recrystallization during LT/HP metamorphism. The relevant PT conditions were estimated to be *ca.* 12 kbar at 300–400 °C (Zhou, 1997; Gao, 2001). The critical mineral assemblages in the meta-mafic enclave and the host meta-plagiogranites have preserved the textures revealing the metamorphic process. The jadeite and rutile inclusions in albite and titanite respectively in the meta-plagiogranites are considered to represent peak-metamorphic conditions. Albite, magnesio-riebeckite, aegirine-augite and the titanite rims of rutile are related to post-peak

Table 5
U–Pb isotopic data obtained by SHRIMP method for zircons from meta-plagiogranite host rocks.

Grain spot	U (ppm)	Th (ppm)	$^{206}Pb^*$ (ppm)	$^{232}Th/^{238}U$	$^{206}Pb_c$ (%)	$^{238}U/^{206}Pb$	±1σ	$^{207}Pb^*/^{206}Pb^*$	±1σ	$^{207}Pb^*/^{235}U$	±1σ	Age (Ma) $^{206}Pb/^{238}U$	±1σ	$^{207}Pb/^{206}Pb$	±1σ	$^{208}Pb/^{232}Th$	±1σ
JX15-4-1.1	104	79	14.6	0.79	4.57	6.456	3.2	0.0708	17	1.51	18	928	27	951	358	870	137
JX15-4-2.1	508	618	12.3	1.26	–	38.52	3.5	0.0125	147	0.045	148	165.2	5.7	–	–	73	22
JX15-4-1.2	106	77	16.1	0.75	1.54	5.9	3.1	0.0513	20	1.198	21	1009	29	253	471	778	128
JX15-4-1.3	168	14	18.5	0.09	4.87	8.365	3.1	0.0524	12	0.864	12	728	22	303	270	–	–
JX15.4-1.4	82	53	11.7	0.67	5.04	6.41	3.3	0.0634	25	1.363	25	935	29	721	522	878	161
JX15-4-3.1	134	124	18.9	0.95	1.81	6.24	2.8	0.067	10	1.481	10	958	25	839	200	927	61
JX15-4-4.1	287	227	41.1	0.82	0.95	6.113	2.6	0.0693	5.8	1.562	6.3	977	24	906	118	905	49
JX15-4-5.1	103	77	11.8	0.77	3.53	8.057	3.4	0.0323	46	0.553	46	754	25	–	–	549	124
JX15-4-4.2	212	32	33.6	0.15	1.56	5.591	2.8	0.0546	12	1.347	12	1061	28	397	262	384	376
JX15-4-6.1	147	101	21	0.71	–	6.16	2.8	0.0616	11	1.378	12	970	25	659	242	448	104
JX15-4-7.1	41	12	6.2	0.3	7.78	7.045	5.6	–	–	–	–	856	45	–	–	–	–
JX15-4-8.1	63	20	8.9	0.32	3.09	6.484	3.5	0.0488	33	1.038	33	925	30	138	764	426	381
JX15-4-9.1	72	28	10.9	0.4	6.48	6.11	3.5	0.0686	24	1.548	24	977	31	887	488	860	322
JX15-4-10.1	171	49	20.1	0.3	1.13	7.572	2.8	0.0618	11	1.126	11	800	21	669	237	383	163
JX15-4-11.1	142	218	13.3	1.59	–	9.816	3.2	0.0503	26	0.706	26	625	19	207	602	227	50

Pb_c Pb* indicate the common and the radiogenic portions respectively; the common Pb corrected using measured ^{204}Pb.

metamorphism. The augite rims of aegirine-augites, the winchite, barroisite and actinolite alteration rims and matrix apatite were the youngest retrograde products. On the other hand, the ilmenite inclusions in rutile and amphibole, the Mg–Fe–Mn amphibole and riebeckite inclusions in albites or aegirine-augites and high anorthite-bearing plagioclase, apatite inclusions in albites possibly represent relics of the former magmatic mineral paragenesis.

Although the mineral modal abundances of the meta-plagiogranite host rocks and the meta-mafic enclave are quite variable (Table 1), their mineral parageneses are similar. Both the meta-mafic enclave and meta-plagiogranite host rocks are interpreted to have had the same primary magmatic mineral paragenesis consisting of plagioclase + hornblende + apatite + monazite + ilmenite + zircon. However, the plagioclase modal amount in the meta-mafic enclave is much lower, while the hornblende and apatite mineral abundances are higher compared with those of the meta-plagiogranite host rocks.

6.2. Generation of the adakitic signature

The enclave-bearing meta-plagiogranite has a chemical composition similar to that of modern adakites (Drummond et al., 1996; Martin, 1999), with high Mg# (53.5) as well as high Al_2O_3 (15.86 wt.%) and Sr (485 ppm) and a positive Eu-anomaly. The high Sr/Y (238) and $(La/Yb)_N$ (35) ratios and low Y and Yb contents (2.33 and 0.210 ppm, respectively) seem to indicate garnet to be a refractory phase. In the $(La/Yb)_N$–Yb_N and Sr–Y diagrams, all meta-plagiogranite host rocks plot into the adakite field (Fig. 10a and b). This is in agreement with the results of Li and Li (2003), who interpreted the adakitic signature to be due to melting of subducted, spilitized oceanic crust at pressures high enough to stabilize garnet and amphibole. The high εNd(970 Ma) between 6.6 and 7.4, supports a MORB source for these meta-plagiogranites (Fig. 8). However, low $^{87}Sr/^{86}Sr$ (0.7026 to 0.7027) precludes melting of subducted, spilitized oceanic crust since altered oceanic crust from both modern oceanic floor and ophiolite suite has higher $^{87}Sr/^{86}Sr$ from 0.70364 to 0.70744 (e.g. Coleman, 1977; Staudigel et al., 1995).

As noted earlier the meta-mafic enclave has low $^{87}Sr/^{86}Sr$ (0.7023) and εNd(970 Ma) (6.2) values similar to those of the meta-plagiogranite host rocks (Fig. 8). This suggests that both the enclave and the host rocks were generated from the same depleted mantle source. Compared with the meta-plagiogranite host rocks, the meta-mafic enclave has a negative Eu anomaly, lower Sr/Y (15) and (La/

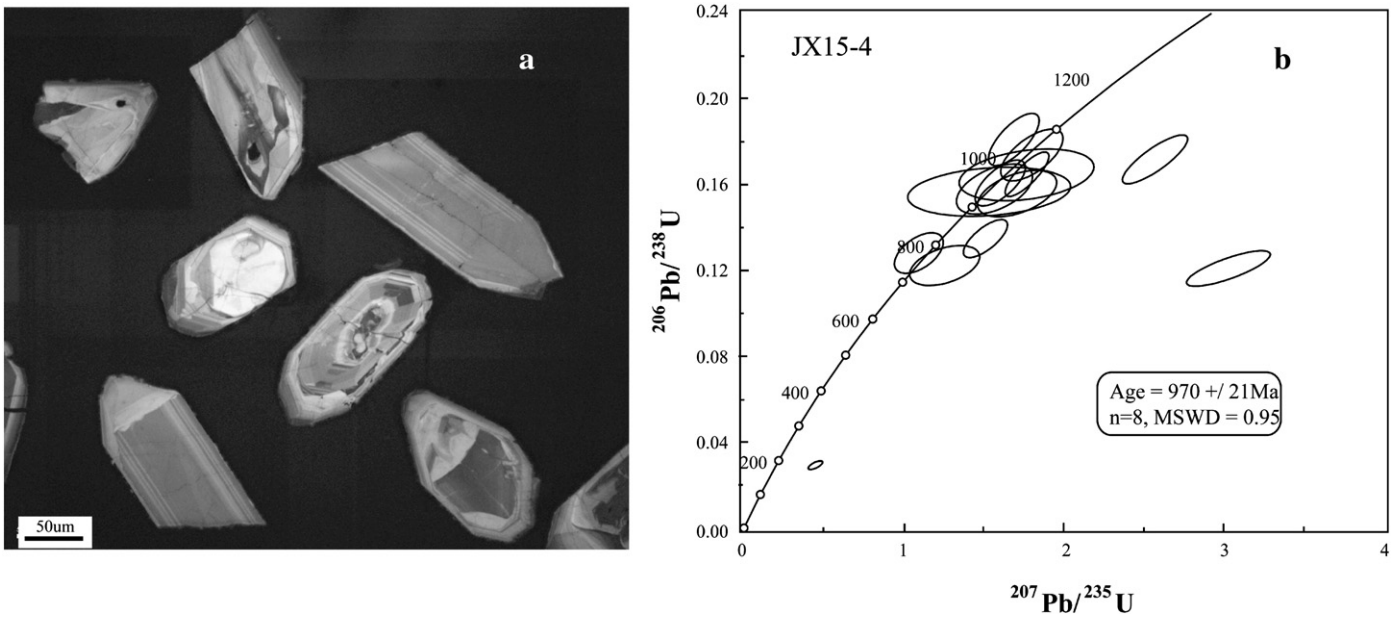

Fig. 9. (a) Representative cathodoluminescence images of zircon grains from the meta-plagiogranite host rocks, (b) U–Pb concordia diagram for zircon grains from the meta-plagiogranite host rocks.

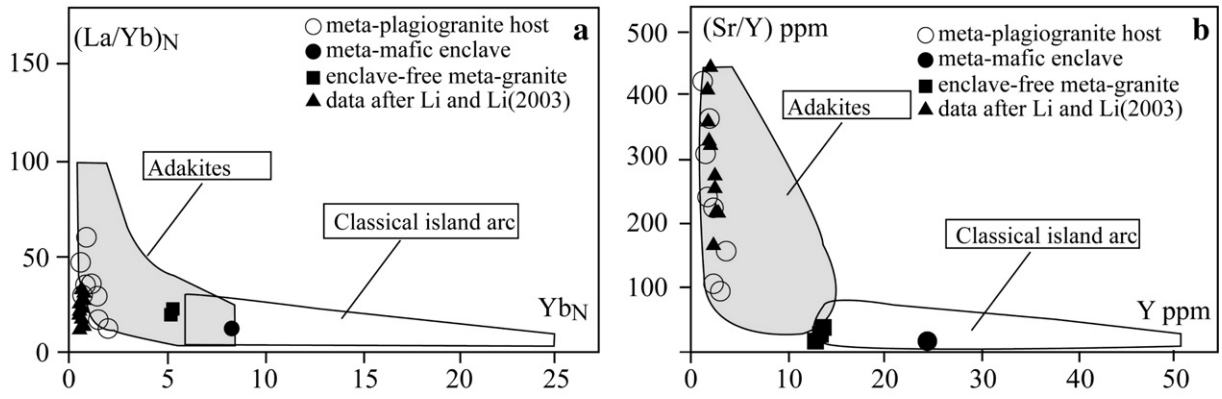

Fig. 10. (La/Yb)N vs. YbN (a; Martin, 1986) and Sr/Y vs. Y (b; Drummond and Defant, 1990) diagrams for the meta-plagiogranite host rocks, the meta-mafic enclave and the enclave-free meta-plagiogranites.

$Yb)_N$ (5) ratios and higher concentrations of all HREEs, and plots into the island arc rock field (Fig. 10a and b). These compositional characteristics are complementary to those of the meta-plagiogranite host rocks, and combined with the similar isotopic signature suggest that these rocks share a genetic relationship with the meta-mafic enclave.

Generally, three types of mafic magmatic enclaves have been recognized in granite intrusions: residues of crustal rock melting (i.e., restite model), cognate segregation (i.e., autolith model) and mafic end-members resulting from magma mixing (i.e., magma mixing model)—(Barbarin and Didier, 1991). The magma mixing model can be excluded in the present study since the mafic-enclave and the meta-plagiogranites were derived from the same source as is indicated by the Sr and Nd isotopic data. Although the generation of the granites through the melting of subducted, spilitized oceanic crust seems to be precluded by the low $^{87}Sr/^{86}Sr$ value, the meta-plagiogranite host rocks could still have been generated by the melting of unaltered oceanic basalts represented by the meta-mafic enclave. However, the major and trace elements of the meta-plagiogranite host rocks and meta-mafic enclave do not display any correlation (Fig. 6) arguing against the restite model (cf. Chappell and White, 1991). In addition, garnet and hornblende have been suggested to represent residual phases during the generation of adakitic magmas related to melting of a basaltic rock at relatively high pressure (e.g. Defant and Drummond, 1990; Martin, 1999). The experimental results on metabasalts further suggest that adakitic magmas are generated by partial melting of a wet mafic protolith in the garnet stability field (e.g., Rapp et al., 1991). The meta-mafic enclave in this study is predominantly composed of recrystallized amphibole, clinopyroxene, titanite and apatite. This mineral assemblage indicates that the meta-mafic enclaves were not generated in the garnet stability field and thus excludes the restite model. In summary, the textural, mineralogical and geochemical data do not support the restite model in which the meta-mafic enclave is the residual phase and the meta-plagiogranite host rock is the product of melting of the oceanic crust.

The isotopic and mineralogical similarity of the mafic-enclave and the host rocks rather suggests a coeval and cognate relationship based on the early crystallization or aggregation of mafic and accessory minerals as in the autolith model (e.g., Barbarin and Didier, 1991). This is further supplemented by the elongated and lenticular shape of the meta-mafic enclaves and their gradational contacts to the host rocks (Fig. 2a), which are very similar to those of typical 'schlieren' (Didier and Barbarin, 1991; Best, 2003). Although the mineral modal abundances of the meta-mafic enclave and the meta-plagiogranite host rocks are variable (Table 1), the metamorphic and the deduced primary magmatic mineral assemblage are similar. Therefore, the meta-mafic enclaves are regarded as schlieren in the meta-plagiogranite host rocks. In summary, the mineralogical, textural and isotopic data support the autolith model for the generation of the meta-mafic enclaves, whereby they resulted from the crystallization of hornblendes and accessory minerals (apatite and ilmenite) from the same magma source of the meta-plagiogranite host rocks (see below).

The unfractionated REE distribution pattern of the meta-mafic enclave and the strongly REE fractionated pattern of host meta-plagiogranites are complementary (Fig. 7a) and indicate that fractional crystallization was involved during the formation of the meta-mafic enclave and the meta-plagiogranite host rocks. The segregation of minerals into the enclave is thought to have caused its HREE and Y enrichment and the corresponding depletion of these elements in the meta-plagiogranite host rocks. Mass balance calculations for Sr, Nb, Y, and Yb are based on the trace element concentrations of the whole rocks and minerals (Sample JX158b; Tables 3 and 4) and the modal amounts of minerals in the enclave (Table 1). The results (Fig. 11) indicate that the Y and Yb are hosted in amphibole, apatite and titanite; Nb in rutile, titanite and amphibole and Sr in plagioclase, amphibole and titanite. For example, Na-amphibole in the meta-mafic enclave displays *ca.* 25% Y and 48% Yb, apatite *ca.* 28% and 19% and titanite *ca.* 37% and 33%. However, Na-amphibole, albite, apatite and titanite in the meta-mafic enclave are metamorphic minerals, which (re)crystallized from the primary magmatic assemblage hornblende + plagioclase + apatite + ilmenite + monazite + zircon during LT–HP metamorphism.

Therefore, the generation of the adakitic signature (i.e., low Y and Yb contents, high Sr/Y and La/Yb ratios) in the enclave-bearing meta-plagiogranites is thought to have been controlled by fractional crystallization of primary magmatic hornblende and apatite/ilmenite from the granitic parent magma. A plagioclase-controlled fractionation would decrease Sr and SiO_2 contents (Castillo et al., 1999; Garrison and Davidson, 2003; Petrone and Ferrari, 2008). The MgO and Ni concentrations of the meta-adakitic granite host rocks are almost constant with increasing SiO_2, indicating that orthopyroxene and olivine were not involved in the fractional crystallization process. Quantitative modeling has been employed to interpret the generation of Quaternary adakitic volcanics from parent basaltic magma (Castillo et al., 1999; Garrison and Davidson, 2003; Petrone and Ferrari, 2008). However, in the present study the investigated rocks have a metamorphic mineral assemblage which makes it impossible to deduce the exact modal amount of primary magmatic minerals or to identify a possible protolith rock.

6.3. Tectonic environments and origin of high-pressure metamorphic rocks

Plagiogranites are usually a minor leucocratic component of most ophiolite complexes (e.g. Coleman, 1977; Floyd et al., 1998) or are exposed as small intrusive bodies spatially related to island-arc

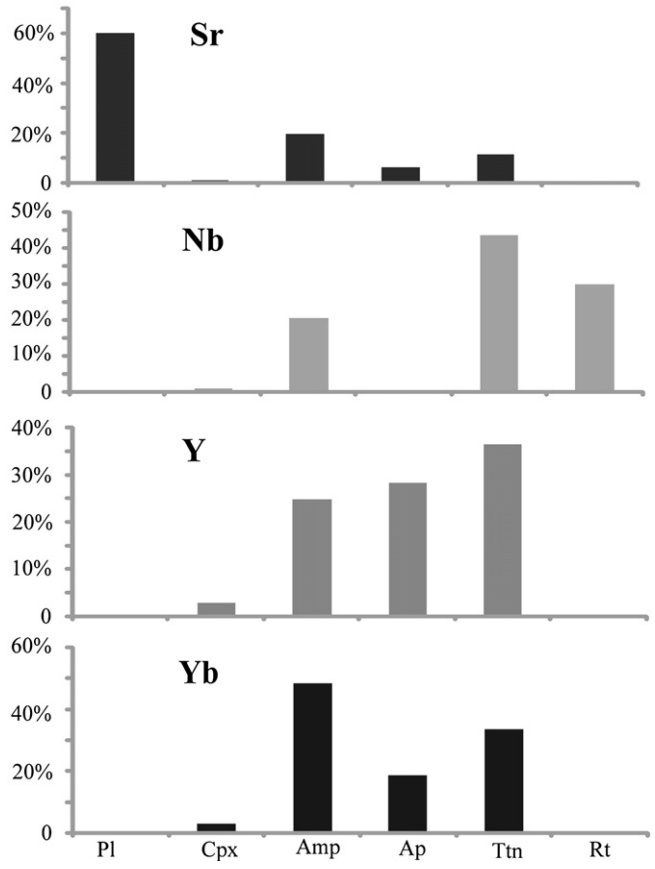

Fig. 11. Diagram showing the mass balance calculation results for Sr, Nb, Y, and Yb of the meta-mafic enclave (Sample JX 158b). Calculation was based on the trace element concentrations of whole rocks (Table 4), average trace element concentrations of minerals (Table 3) and modal abundance of minerals (Table 1).

granitoids in the axial part of volcanic arcs (e.g. Pavlis et al., 1988; Maeda and Kagami, 1996; Luchitskaya et al., 2005). The former usually occur as veins, dykes or small bodies and always show an intimate relationship with the surrounding gabbros, sheeted diabase dykes or pillow lavas and breccias (Bebien, 1991; Floyd et al., 1998). The latter usually intrude into other granitoids, volcanic rocks or sedimentary sequences of an island-arc volcanic belt (e.g. Luchitskaya et al., 2005). Li and Li (2003) negated the possibility that the Xiwan meta-plagiogranites were formed by extensive fractional crystallization of a basaltic magma as a leucocratic component of ophiolite complexes (e.g., Floyd et al., 1998). They further dismissed a generation related to anatexis of amphibolites near a spreading center as shear-type granites (Pedersen and Malpas, 1984) or of the sedimentary rocks beneath ophiolite thrust sheets as obduction-type granites (Skjerlie et al., 2000).

Various kinds of exotic blocks comprising a gabbroic, MORB-type basaltic, island-arc type basaltic diabasic, dioritic and chert-like composition are present in the NE Jiangxi ophiolitic mélange, (Zhou, 1989; Shu and Zhou, 1988; Shu et al., 1995; Chen et al., 1991; Xu et al., 1992; Li et al., 1997). In addition high-pressure adakitic meta-plagiogranite (Zhou, 1997; Li and Li, 2003), meta-non adakitic plagiogranite and obduction-type leucogranitic blocks (Li et al., 2008) were reported from this locality. Although the formation of the meta-plagiogranite protoliths took place in the Neoproterozoic (at *ca.* 970 Ma; Li et al., 1994 and this study), the formation of the mélange belt is poorly constrained. The *ca.* 880 Ma obduction-type granites may provide a petrological constraint on the timing of the ophiolite obduction onto the continental crust (Li et al., 2008). It should be noted that the Xiwan high-pressure meta-plagiogranite may have been introduced into the serpentinite matrix after high-pressure metamorphism (at *ca.* 866–799 Ma; Hu et al., 1993; Shu et al., 1994). The generation of the plagiogranites cannot be related to the ophiolite suite since no gabbros, sheeted diabase dykes or pillow lavas and breccias were observed as country rocks of the meta-plagiogranites. In addition, the structure of the meta-mafic enclaves and the meta-plagiogranite host rocks differs from that of the enclaves occurring in typical ophiolitic plagiogranite (Bebien, 1991).

As discussed earlier, the enclave-free meta-plagiogranite plots into the field of classic island arc rocks in the Sr–Y diagram (Fig. 10b). Their high $^{87}Sr/^{86}Sr$ ratios (0.7037–0.7045) and $\varepsilon Nd(970\ Ma)$ values (−1.22 to −1.28) suggest significant crustal reworking or contamination by subducted sediments, continental crusts, or fluids derived from the dehydration of sediments. Both the enclave-free meta-plagiogranites and the meta-plagiogranite host rocks are volcanic arc-type granite in the Rb–Y + Nb and Nb–Y diagram (Fig. 12; Pearce et al., 1984). The $^{87}Sr/^{86}Sr$ ratios and $\varepsilon Nd(970\ Ma)$ values of the meta-mafic enclave and the meta-plagiogranite host rocks indicate the generation from a depleted mantle source without a contribution from continental components. The upper mantle wedge beneath the Neoproterozoic island arc along the southern margin of Yangtze block (Li et al., 1997) may be a suitable source for the generation of the parent basaltic magmas for these rocks. During the ascent of such magmas, fractional crystallization of hornblende and accessory minerals such as apatite may have controlled the decrease of Y and Yb concentrations in certain parts of the magma and thereby created the adakitic signature of its host rock (i.e. enclave-bearing meta-plagiogranite).

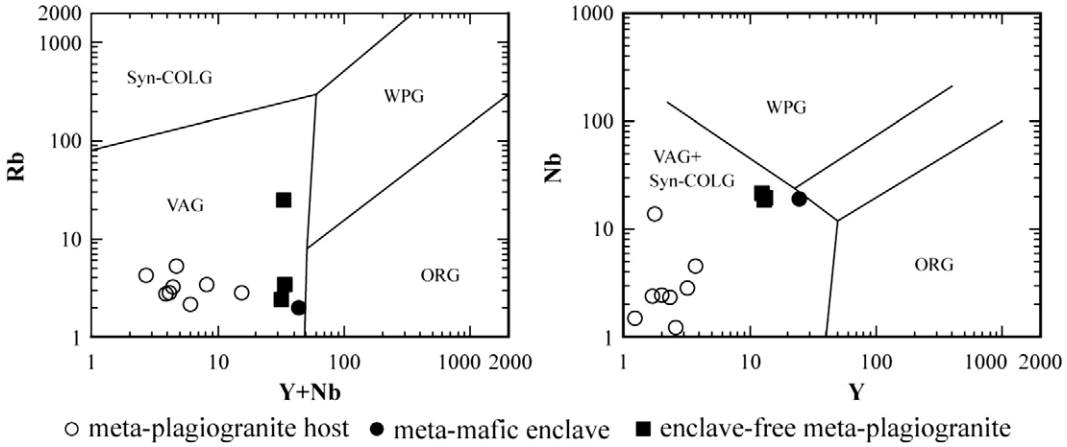

Fig. 12. Tectonic discrimination diagrams for the meta-plagiogranite host, the meta-mafic enclave and the enclave-free meta-plagiogranite (Pearce et al., 1984). Y + Nb vs. Rb (a) and Y vs. Nb (b).

7. Conclusion

1. The high-pressure metamorphic rocks which are exposed within the NE Jiangxi ophiolitic mélange consist of enclave-bearing and -free meta-plagiogranites.
2. The enclave-bearing meta-plagiogranite host rock has a chemical composition similar to that of modern adakites with high Al_2O_3 and Sr contents as well as a high Mg number. Strongly fractionated REE pattern ($(La/Yb)_N > 12$) are associated with low Y and Yb concentrations and a positive Eu-anomaly. The meta-mafic enclave has a basaltic composition with higher concentrations of REEs and Y. The composition of the enclave-free meta-plagiogranite resembles that of classic island arc rocks. Both the mafic enclave and the meta-plagiogranite host rocks have low $^{87}Sr/^{86}Sr$ and $\varepsilon Nd(970\ Ma)$ values indicating derivation from a depleted mantle source. The enclave-free meta-plagiogranite has relatively higher $^{87}Sr/^{86}Sr$ and negative $\varepsilon Nd(970\ Ma)$ values suggesting contamination by continental crust.
3. The meta-mafic enclaves are interpreted to represent 'schlieren' which were formed by early fractional crystallization of accessory minerals and hornblende, thereby generating the adakitic signature in the meta-plagiogranite host rocks.
4. The granitic magma was derived from a basaltic parental melt generated from the mantle wedge beneath the Neoproterozoic island arc along the southern margin of Yangtze block. Therefore, adakitic rocks may be produced by means of fractional differentiation of island arc basaltic magmas.

Acknowledgements

This research was supported by the National Natural Science Foundation of China (40721062), 'Funds for Youth Geologist' sponsored by Former Ministry of Geology and Mineral Resources (Qn979824), 'Funds for Hundred Outstanding Talents Plan' sponsored by Chinese Academy of Sciences. We are indebted to R. Baur for the XRF-analyses, X. D. Jin and H. Y. Li for the trace element analysis, B. Song and H. Tao for the SHRIMP dating, H. Brätz for the LA-ICP-MS analyses, Y. G. Ma and Q. Mao for electron microprobe analyses and Z. Y. Chu and S. H. Tang for the isotope analyses. The authors appreciate discussions with X. H. Li, F. Y. Wu, B. F. Han, W. Liu, V. von Seckendorf and T. John and support from S. L. Shu and B. Xu for conducting this study. Furthermore we highly appreciate the constructive reviews by P. R. Castillo, C. M. Petrone and N. Eby which significantly improved the manuscript.

References

Atherton, M.P., Petford, N., 1993. Generation of sodium-rich magmas from newly underplated basaltic crust. Nature 362, 144–146.
Black, L.P., Kamo, S.L., Allen, C.M., Aleinikoff, J.N., Davis, D.W., Korsch, R.J., Roudoulis, C., 2003. TEMORA 1: a new zircon standard for Phanerozoic U–Pb geochronology. Chemical Geology 200, 155–170.
Barbarin, B., Didier, J., 1991. Review of the hypotheses proposed for the genesis and evolution of mafic microgranular enclaves. In: Didier, J., Barbarin, B. (Eds.), Enclaves and Granite Petrology. Elsevier Science Publisher B.V., Amsterdam, pp. 367–373.
Bebien, J., 1991. Enclaves in plagiogranites of the Guevgueli ophiolitic complex, Macedonia, Greece. In: Didier, J., Barbarin, B. (Eds.), Enclaves and Granite Petrology. Elsevier Science Publisher B.V., Amsterdam, pp. 205–219.
Best, M.G., 2003. Igneous and Metamorphic Petrology. Blackwell Publishing, p. 176.
Castillo, P., 2006. An overview of adakite petrogenesis. Chinese Science Bulletin 51, 257–268.
Castillo, P.R., Janney, P.E., Solidum, R.U., 1999. Petrology and geochemistry of Camiguin Island, southern Philippines: insights to the source of adakites and other lavas in a complex arc setting. Contribution to Mineralogy and Petrology 134, 33–51.
Chappell, B.W., White, A.J.R., 1991. Restite enclaves and the restite model. In: Didier, J., Barbarin, B. (Eds.), Enclaves and Granite Petrology. Elsevier Science Publisher B. V., Amsterdam, pp. 375–381.
Chen, J., Foland, K.A., Xing, F., Xu, X., Zhou, T., 1991. Magmatism along the southeastern margin of the Yangtze block: Precambrian collision of the Yangtze and Cathaysia blocks of China. Geology 19, 815–818.
Coleman, R.G., 1977. Ophiolites: Ancient Oceanic Lithosphere? Springer-Verlag, Berlin Heidelberg, p. 229.
Defant, M.J., Drummond, M.S., 1990. Derivation of some modern arc magmas by melting of young subducted lithosphere. Nature 347, 662–665.
Didier, J., Barbarin, B., 1991. The different types of enclaves in granites—nomenclature. In: Didier, J., Barbarin, B. (Eds.), Enclaves and Granite Petrology. Elsevier Science Publisher B. V., Amsterdam, pp. 19–23.
Drummond, M.S., Defant, M.J., 1990. A model for trondhjemite–tonalite–dacite genesis and crustal growth via slab melting: Archaean to modern comparisons. Journal of Geophysics Research 95, 21503–21521.
Drummond, M.S., Defant, M.J., Kepezhinskas, P.K., 1996. The petrogenesis of slab derived rondhjemite–tonalite–dacite–adakite magmas. Transactions of the Royal Society of Edinburgh: Earth Science 87, 205–215.
Floyd, P.A., Yalinitz, M.K., Goncuoglu, M.C., 1998. Geochemistry and petrogenesis of intrusive and extrusive ophiolitic plagiogranites, Central Anatolian Crystalline Complex, Turkey. Lithos 42, 225–241.
Gao, J., 2001. Rock types, mineral constituents and metamorphic process of high-pressure metamorphic rocks in Northeastern Jiangxi province. Acta Petrologica et Mineralogica 20, 134–145 (in Chinese with English Abstract).
Garrison, J.M., Davidson, J.P., 2003. Dubious case for slab melting in the Northern volcanic zone of the Andes. Geology 31, 565–568.
Gutscher, M., Maury, R., Eissen, J., Bourdon, E., 2000. Can slab melting be caused by flat subduction? Geology 28, 535–538.
He, K.Z., Zhao, C.H., Tai, D.Q., Nie, Z.T., Yue, C.S., Zhou, Z.G., Ye, N., 1996. Discovery of Late Paleozoic Radiolaria silicolite in many places in Northeastern Jiangxi ophiolitic mélange belt. Geoscience 10, 303–307 (in Chinese with English Abstract).
He, K.Z., Zhao, C.H., Yue, C.S., Zhou, Z.G., Nie, Z.T., Tai, D.Q., Ye, N., 1999. Reexamination and impression on "Banxi Group". Earth Science Frontiers 6, 353–362 (in Chinese with English Abstract).
Hsu, K.J., Sun, S., Li, J.L., Chen, H.H., Pen, H.P., Sengor, A.M.C., 1988. Mesozoic overthrust tectonics in South China. Geology 16, 418–421.
Hu, S.L., Zhou, H.P., Zhou, X.M., 1993. The $^{40}Ar/^{39}Ar$ ages for crosstie from the albite granite in Dexing of Jiangxi province and for muscovite from the cordierite granite in Shexian of Anhui province and their geological significance. In: Li, J.L. (Ed.), The Structure of Continental Lithosphere and Tectonic Evolution of SE China. Metallurgical Industry Publishing House, Beijing, pp. 141–144 (in Chinese).
Kleinhanns, I., Kramers, J., Kamber, B., 2003. Importance of water for Archaean granitoid petrology: a comparative study of TTG and potassic granitoids from Barberton Mountain Land, South Africa. Contribution to Mineralogy and Petrology 145, 377–389.
Leake, B.E., 1997. Nomenclature of amphiboles. European Journal of Mineralogy 9, 623–651.
Li, W.X., Li, X.H., 2003. Adakitic granites within the NE Jiangxi ophiolites, South China: geochemical and ND isotopic evidence. Precambrian Research 122, 29–44.
Li, X.H., Zhou, G.Q., Zhao, J.X., Fanning, C.M., Compston, W., 1994. SHRIMP ion probe zircon age of the NE Jiangxi Ophiolite and its tectonic implications. Geochimca 23, 117–123 (in Chinese with English Abstract).
Li, X.H., Zhao, J.X., McCulloch, M.T., Zhou, G.Q., Xing, F.M., 1997. Geochemical and Sm–Nd isotopic study of Neoproterozoic ophiolites from southeastern China: petrogenesis and tectonic implications. Precambrian Research 81, 129–144.
Li, Z.X., Cho, M., Li, X.H., 2003. Precambrian tectonics of East Asia and relevance to supercontinent evolution. Precambrian Research 122, 1–6.
Li, Z.X., Evans, D.A.D., Zhang, S., 2004. A 90 spin on Rodinia: possible causal links between the Neoproterozoic supercontinent, superplume, true polar wander and low-latitude glaciation. Earth and Planetary Science Letters 220, 409–421.
Li, W.X., Li, X.H., Li, Z.X., Lou, F.S., 2008. Obduction-type granites within the NE Jiangxi Ophiolite: implications for the final amalgamation between the Yangtze and Cathaysia Blocks. Gondwana Research 13, 288–301.
Luchitskaya, M.V., Morozov, O.L., Palandzhyan, S.A., 2005. Plagiogranite magmatism in the Mesozoic island-arc structure of the Pekulney Ridge, Chukotka Peninsula, NE Russia. Lithos 79, 251–269.
Ludwig, K.R., 1991. Isoplot: a plotting and regression program for radiogenic-isotope data. US Geological Survey Open-File Report 39.
Macpherson, C.G., Dreher, S.T., Thirlwall, M.F., 2006. Adakites without slab melting: high pressure differentiation of island arc magma, Mindanao, the Philippines. Earth and Planetary Science Letters 243, 581–593.
Maeda, J., Kagami, H., 1996. Interaction of a spreading ridge and an accretionary prism: implications from MORB magmatism in the Hidaka magmatic zone, Hokkaido. Geology 24, 31–34.
Martin, H., 1986. Effect of steeper Achaean geothermal gradient on geochemistry of subduction-zone magmas. Geology 14, 753–756.
Martin, H., 1999. Adakitic magmas: modern analogues of Archean granitoids. Lithos 46, 411–429.
Middlemost, E.A.K., 1994. Naming materials in the magma/igneous rocks system. Earth Science Reviews 37, 215–224.
Morimoto, N., 1988. Nomenclature of pyroxenes. American Mineralogist 73, 1123–1133.
Pavlis, T.L., Monteverde, D.H., Bowman, J.R., Rubenstone, J.L., Reason, M.D., 1988. Early Cretaceous near-trench plutonism in Southern Alaska: a tonalite-trondhjemite intrusive complex injected during ductile thrusting along the Border Ranges fault system. Tectonics 7, 1179–1199.
Pearce, J.A., Harris, N.B.W., Tindle, A.G., 1984. Trace element discrimination diagrams for the tectonic interpretation of granitic rocks. Journal of Petrology 25, 956–983.
Pedersen, R.B., Malpas, J., 1984. The origin of oceanic plagiogranites from the Karmoy ophiolite, Western Norway. Contribution to Mineralogy and Petrology 88, 36–52.
Petrone, C.M., Ferrari, L., 2008. Quaternary adakite–Nb-enriched basalt association in the western Trans-Mexican Volcanic Belt: is there any slab melt evidence? Contribution to Mineralogy and Petrology 156, 73–86.

Prouteau, G., Scaillet, B., 2003. Experimental constraints on the origin of the 1991 Pinatubo dacite. Journal of Petrology 44, 2203–2241.
Qian, Q., Gao, J., Klemd, R., He, G., Xiong, X.M., Long, L.L., Liu, D.Y., Xu, R.H., 2008. Early Paleozoic tectonic evolution of the Chinese South Tianshan Orogen: constraints from SHRIMP zircon U–Pb geochronology and geochemistry of basaltic and dioritic rocks from Xiate, NW China. International Journal of Earth Sciences. doi:10.1007/s00531-007-0268-x.
Rapp, R.P., Watson, E.B., Miller, C.F., 1991. Partial melting of amphibolite/eclogite and the origin of Archaean trondhjemites and tonalites. Precambrian Research 51, 1–25.
Rodriguez, C., Selles, D., Dungan, M., Langmuir, C., Leeman, W., 2007. Adakitic dacite formed by intracrustal crystal fractionation of water-rich parent magmas at Nevado de Longavi Volcano (36.2°S; Andean Southern Volcanic Zone, Central Chile). Journal of Petrology 48, 2033–2061.
Rowley, D.B., Ziegler, A.M., Gyou, N., 1989. Comment on "Mesozoic overthrust tectonics in South China". Geology 17, 384–386.
Sajona, F.G., Maury, R.C., Bellon, H., Cotten, J., Defant, M.J., Pubellier, M., 1993. Initiation of subduction and the generation of slab melts in western and eastern Mindanao, Philippines. Geology 21, 1007–1010.
Shu, L.S., Zhou, G.Q., 1988. The first discovery of the high-pressure minerals in the collage zone of Proterozoic terrains in north Jiangxi and its tectonic significance. Journal of Nanjing University 24, 421–429.
Shu, L.S., Zhou, G.Q., Shi, Y.S., Yin, J., 1994. Study on the high-pressure metamorphic blueschist and its Late Proterozoic age in the eastern Jiangnan belt. Chinese Science Bulletin 39, 1200–1204.
Shu, L.S., Shi, Y.S., Guo, L.Z., Charvet, J., Sun, Y., 1995. Plate tectonic evolution and the kinematics of collisional orogeny in the Middle Jiangnan, eastern China. Publishing House of Nanjing University, pp. 122–139.
Skjerlie, K.P., Pedersen, R.B., Wennberg, O.P., De La Rosa, J., 2000. Volatile phase fluxed anatexis of sediments during late Caledonian ophiolite obduction: evidence from the Sogneskollen Granitic Complex, West Norway. Journal of Geological Society London 157, 1199–1213.
Staudigel, H., Davies, G.R., Hart, S.R., Marchant, K.M., Smith, B.M., 1995. Large scale isotopic Sr, Nd and O isotopic anatomy of altered oceanic crust: DSDP/ODP sites 417/418. Earth and Planetary Science Letters 130, 169–185.
Taylor, S.R., McLennan, S.M., 1985. The Continental Crust: Its Composition and Evolution. Blackwell, Oxford.
Thorkelson, D.J., Breitsprecher, K., 2005. Partial melting of slab window margins: genesis of adakitic and non-adakitic magmas. Lithos 79, 25–41.
White, W.M., 2007. Geochemistry. John-Hopkins University Press, pp. 313–358.
Xiao, W.J., He, H.Q., 2005. Early Mesozoic thrust tectonics of the northwest Zhejiang region (Southeast China). Geological Society of American Bulletin 117, 945–961.
Xu, B., Qiao, G.S., 1989. Sm–Nd isotopic age of the late Proterozoic ophiolite suite in NE Jiangxi province and its primary tectonic environment. Journal of Nanjing University (Earth Sciences) 1, 108–114 (in Chinese with English abstract).
Xu, B., Guo, L.Z., Shi, Y.S., 1992. Proterozoic Terranes and Multiphase Orogens in the Anhui-Jiangxi Area. Geological Publishing House, Beijing. 112 pp. (in Chinese with English abstract).
Yogodzinski, G.M., Kelemen, P.B., 1998. Slab melting in the Aleutians: implications of an ion probe study of clinopyroxene in primitive adakite and basalt. Earth and Planetary Science Letters 158, 53–65.
Yogodzinski, G., Lees, J., Churikova, T., Dorendorf, F., Woerner, G., Volynets, O., 2001. Geochemical evidence for the melting of subducting oceanic lithosphere at plate edges. Nature 409, 500–504.
Zhao, J.X., Li, X.H., McCulloch, M.T., Zhou, G.Q., Xing, F.M., 1995a. Petrogenesis of ophiolites from South Abhui and Northeast Jiangxi, and their tectonic implications: chemical and Sm–Nd isotopic constraints. Geochimca 24, 311–326 (in Chinese with English Abstract).
Zhao, C.H., He, K.Z., Mao, X.X., Tai, D.Q., Ye, D.L., Ye, N., Lin, P.Y., Bi, X.H., Zheng, B.R., Feng, Q.I., 1995b. The discovery of late Paleozoic Radiolaria-bearing cherts within the ophiolite mélanges along the NE Jiangxi Fault Zones and its implications. Chinese Science Bulletin 40, 2161–2163.
Zhao, C.H., He, K.Z., Tai, D.Q., Le, C.S., Nie, Z.T., Ye, N., 1997. $^{40}Ar/^{39}Ar$ ages of major igneous rocks in Northeastern Jiangxi province. Earth Science 22, 257–260 (in Chinese with English Abstract).
Zhao, Z.H., Xiong, X.L., Wang, Q., Wyman, D.A., Bao, Z.W., Bai, Z.H., Qiao, Y.L., 2008. Underplating related adakites in Xinjiang Tianshan, China. Lithos 102, 374–391.
Zhou, G.Q., 1989. The discovery and significance of the northeastern Jiangxi Province ophiolite (NEJXO), its metamorphic peridotite and associated high-temperature high-pressure metamorphic rocks. Journal of Southeast Asian Earth Science 3, 237–247.
Zhou, G.Q., 1997. Jadeitic rocks from high-pressure metamorphic zone of NE Jiangxi province: formation and preservation condition. Science in China Series D 27 (1), 45–51 (in Chinese with English abstract).
Zhou, G.Q., Zhao, J.X., 1991. Sm–Nd isotopic systematics of the NE Jiangxi ophiolite (NEJXO), SE Margin of the Yangtze craton, South China. Chinese Science Bulletin 36, 1374–1379.